BNL-228431-2025-JAAM

Bridging Structural and Chemical Insights: Integrating In Situ Electron Microscopy and X-ray Spectroscopy for Catalysis Research

Y. Wu, J. Yang

To be published in "The Journal of Physical Chemistry Letters"

June 2025

Center for Functional Nanomaterials

Brookhaven National Laboratory

U.S. Department of Energy

USDOE Office of Science (SC), Basic Energy Sciences (BES). Scientific User Facilities (SUF)

DISCLAIMER

Bridging Structural and Chemical Insights: Integrating in-situ electron microscopy and X-ray spectroscopy for Catalysis Research

Yupeng Wu[1†], Jianyu Wang[1†], Xiaobo Chen[1], Judith C. Yang[2], Guangwen Zhou[1]*

[1]Department of Mechanical Engineering and Materials Science and Engineering Program, State University of New York at Binghamton, New York, 13902

[2]Center for Functional Nanomaterials, Brookhaven National Laboratory, Upton, NY 11973

[†] These authors contributed equally to this work.

Corresponding Author: gzhou@binghamton.edu

ABSTRACT: Environmental transmission electron microscopy probes local structure, composition, and chemistry of materials under gas environments, while ambient-pressure X-ray photoelectron spectroscopy provides ensemble chemical and electronic structure information in gaseous conditions. Both techniques utilize similar differential pumping schemes to mitigate electron scattering by the gas phase, allowing for unique opportunities to correlate gas-surface interactions across comparable pressure ranges. Their integration has advanced the understanding of various catalytic reactions, including the water-gas-shift reaction, CO oxidation, and surface passivation dynamics. The review discusses their methodological advancements, challenges, and potential for further integration with other in situ techniques to address complex catalytic phenomena and guide catalyst design.

TOC Graphic

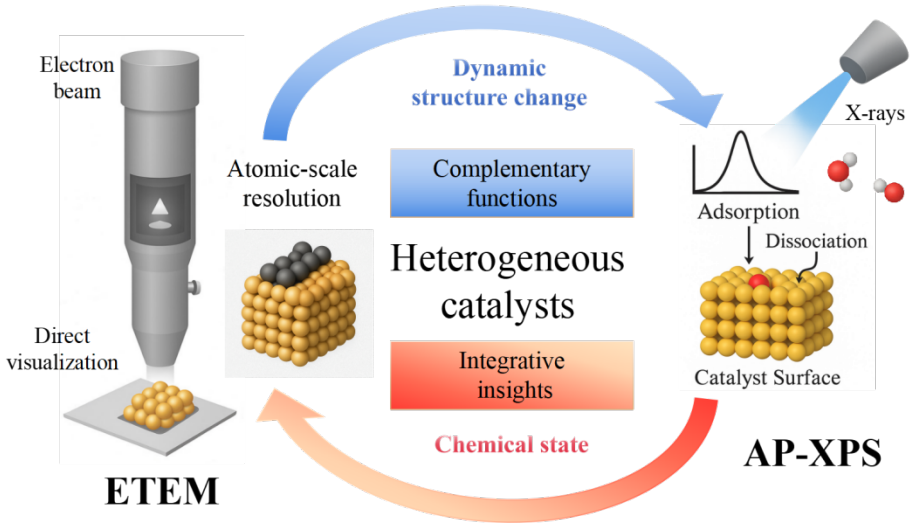

Heterogeneous catalysts are indispensable in chemical processes, energy conversion, and environmental protection, serving as cornerstones for addressing pressing scientific and technological challenges.[1-3] A thorough understanding and effective optimization of their catalytic performance are pivotal for advancing innovation in these domains.[4-8] However, heterogeneous catalytic processes are inherently complex, involving intricate interfacial reactions, dynamic evolution of active sites, adsorption and dissociation of reactants, and desorption of reaction products. Consequently, achieving a holistic understanding of catalyst activity, functionality, and stability remains a formidable yet critical challenge.[9-12]

In recent years, the rapid advancement of in-situ and operando characterization techniques has revolutionized heterogeneous catalysis research. These techniques facilitate real-time monitoring of structural and chemical state changes in catalysts under realistic reaction conditions, providing direct evidence to uncover catalytic mechanisms and performance.[13-18] Among these methods, Environmental Transmission Electron Microscopy (E-TEM) and Ambient Pressure X-ray Photoelectron Spectroscopy (AP-XPS) have emerged as essential tools due to their exceptional spatial resolution and high surface sensitivity.[19-22]

TEM achieves atomic-scale resolution, enabling direct visualization of dynamic structural changes in catalysts during catalytic reactions in gas environments. This includes the reconstruction of metal nanoparticles (NPs),[23] the behavior of active sites in single-atom catalysts, and the interactions at metal-support interfaces.[24] Meanwhile, AP-XPS provides unparalleled insights into the chemical states of catalyst surfaces and subsurfaces under reaction conditions, elucidating mechanisms such as reactant adsorption, dissociation, and intermediate formation.[25,26] Together, these two techniques complement each other by bridging the gap between high spatial resolution and surface chemical sensitivity under comparable pressure conditions, offering a comprehensive framework for investigating the dynamic behavior of heterogeneous catalysts.

This review examines the integration of E-TEM and AP-XPS for in-situ studies of gas-surface reactions, with a particular emphasis on heterogeneous catalysis. It highlights how these techniques complement each other, enhancing our understanding of catalyst activity, functionality, and stability. The review begins with an overview to the working principles of E-TEM and AP-XPS, followed by a summary of their recent applications in studying gas-surface reactions over the past few years. It then discusses the integration of these techniques to investigate the dynamic structural evolution and surface chemical behavior of catalysts. By synthesizing these insights, this review aims to highlight the potential of combining these tools, uncovering fundamental mechanisms of gas-surface reactions with significant implications for the development of high-performance catalysts.

E-TEM has emerged as a powerful in-situ/operando tool for atomic- and nanoscale visualization of catalysts during reactions, providing crucial insights into their structural dynamics under varying gaseous and environmental conditions. Several comprehensive and review articles have highlighted E-TEM methodologies and their applications in catalytic research.[22,27-42] These reviews have explored critical advancements in E-TEM, including its role in understanding catalyst structural evolution in response to controlled gaseous

environments and its contribution to mechanistic insights into catalytic activity. They have also provided in-depth discussions on the design of reaction cells, catalyst synthesis methods, and the characterization of catalytic processes, which collectively support the exploration of structure–property relationships and catalytic mechanisms.

A key challenge in E-TEM lies in introducing reactive gases into the sample region while minimizing their impact on the microscope's vacuum system. To address this, two primary gas introduction strategies have been developed, each with distinct advantages and limitations. The first strategy involves a differential pumping system, which incorporates pressure-limiting apertures within the pole piece and employs turbomolecular and ion getter pumps to achieve gas pressures up to 1.33×10^{-2} bar in the sample region, while maintaining ultra-high vacuum (UHV) near the electron source (Figure 1a-b).[43,44] The advantage of this approach is that it preserves high spatial resolution (sub-Å) by minimizing electron scattering. However, this method is limited by the relatively low gas pressure that can be achieved in the reaction region, which may not always represent realistic operating conditions, particularly for high-pressure reactions. Another disadvantage of this open-cell strategy is its incompatibility with standard TEM setups, requiring significant redesign of the TEM column to accommodate the necessary pumping and pressure control mechanisms.

The second strategy employs specially designed sealed sample holders, where catalyst specimens are enclosed within reaction cells equipped with electron-transparent windows, allowing gas pressures up to atmospheric levels (Figure 1c).[45] This approach provides a clearer understanding of catalyst behavior in environments that more closely mimic industrial processes, where high-pressure conditions are often essential. One key advantage of this method is its compatibility with standard TEM setups, as it does not require extensive redesign of the TEM column. The sealed sample holders can be easily integrated into existing TEM systems, making this approach more accessible and cost-effective compared to the differential pumping strategy. However, one of the main drawbacks of this method is that the enclosed reaction cells can introduce limitations in terms of spatial resolution and sample stability, particularly when high-energy electron beams are used. The electron-transparent windows must be carefully chosen to balance transparency with the ability to withstand harsh reaction conditions, such as high temperature and reactive gases. Furthermore, although the approach is compatible with standard TEM systems, the reaction cells still require some customization to ensure they can accommodate the specific experimental conditions, which may complicate the setup. Despite these challenges, the sealed sample holder strategy offers a powerful and practical solution for studying reactions under high-pressure conditions while maintaining broader compatibility with existing TEM instruments.

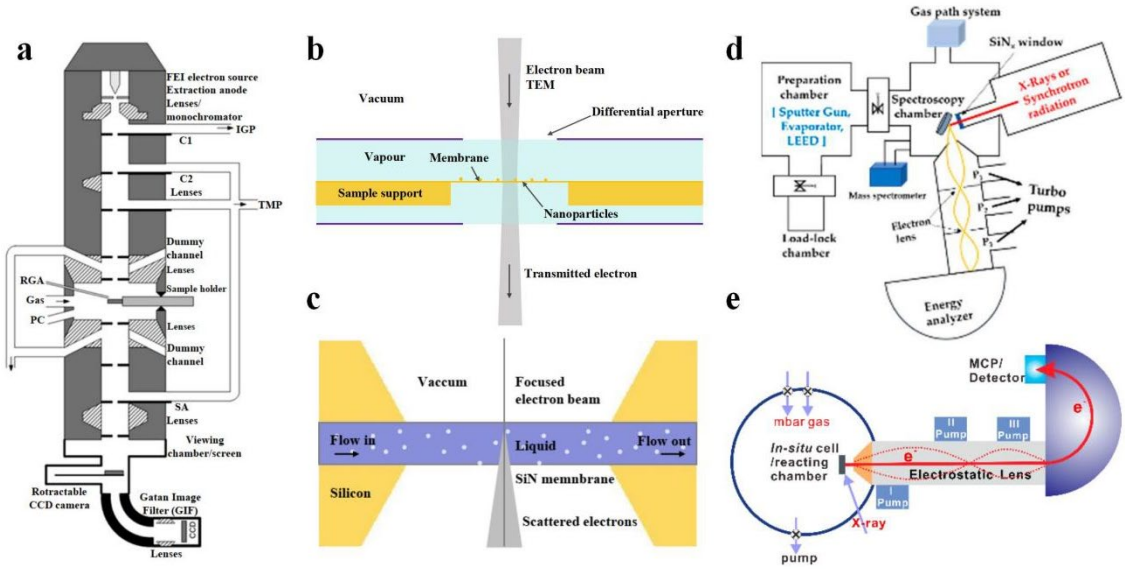

Figure 1. (a) Schematic of an in-situ TEM setup equipped with differential pumping apertures and multi-stage pumps. Adapted from ref 43. *Copyright 2012, Elsevier Ltd. All rights reserved.* (b) Illustration of an open environmental cell containing liquid and vapor, with differential apertures separating the higher sample pressure from the microscope vacuum. Adapted from ref 44. *Copyright 2011, Springer Nature Limited.* (c) Schematic of a closed environmental cell within a TEM sample holder, composed of solid electron-transparent membranes. Adapted from ref 45. *Copyright 2010, Microscopy Society of America.* (d) Diagram of the setup of APXPS. (e) Principles of ambient pressure X-ray photoelectron spectroscopy (XPS) with differential pumping systems. Adapted from ref 58. *Copyright 2019 by the authors.*

The key advantage of E-TEM lies in its ability to conduct high-resolution TEM imaging and electron energy loss spectroscopy (EELS), allowing for the direct observation of structural and chemical changes in catalysts at the nanometer scale and beyond. This unique capability allows researchers to study the dynamic behavior of catalysts under realistic reaction conditions in unprecedented detail. For example, E-TEM has been employed to visualize particle sintering and morphological transformations in noble metal and alloy catalysts,[46-49] oxygen vacancy dynamics,[50-53] and the real-time interfacial reactions occurring in heterogeneous catalytic processes.[54-57]

AP-XPS has gained prominence as a powerful technique in catalysis and electrocatalysis research, owing to its exceptional surface sensitivity, elemental specificity, and operando compatibility.[58-64] Unlike conventional XPS performed under UHV, AP-XPS enables direct, real-time observation of chemical state evolution at catalyst surfaces under near-practical reaction conditions, offering critical insights into the nature and dynamics of active sites. From an instrumentation standpoint, continuous advancements in synchrotron light sources, differential pumping systems, and high-resolution energy analyzers have significantly improved AP-XPS performance, the schematic of its setup and differential pumping systems are shown in Fig. 1d-e.[58] These developments have expanded the accessible pressure range to tens of torr, enhanced time resolution, and enabled the detection of rapid surface chemical transformations—facilitating in situ and operando studies of catalytic kinetics.

AP-XPS offers several distinct advantages, including the ability to precisely measure the valence states and chemical environments of surface elements, thus revealing redox cycles and intermediate species formation at active sites during catalytic reactions.[65-67] By adjusting the probing depth of photoelectrons, AP-XPS can differentiate between the chemical states of surface and subsurface regions, providing crucial information for studying adsorption, dissociation, and interfacial reactions.[25,68-70] Additionally, with the integration of fast scanning and data acquisition technologies, researchers can monitor rapid catalytic reactions in real time. For instance, in photocatalytic and photoelectrocatalytic systems, AP-XPS can identify binding energy shifts of key elements, elucidating charge transfer mechanisms at the interface between cocatalysts and semiconductors, and offering insights into electron-hole separation processes.[21]

AP-XPS and E-TEM are indispensable tools in heterogeneous catalysis research, but each comes with inherent limitations that can hinder a comprehensive understanding of catalytic processes. AP-XPS provides detailed chemical insights into catalyst oxidation states, reaction intermediates, and surface chemical changes on the ensemble scale, with a probing area ranging from a few hundred micrometers to millimeters. However, its limited spatial resolution restricts direct observation of local chemical transformations during catalytic reactions.[21,58,71-76] Conversely, E-TEM excels at capturing local structural dynamics and morphological changes at the nanometer scale and below. However, it lacks the ability to directly probe chemical states of active sites or the molecular characteristics of reaction products.[77-79]

A key consideration is the necessity of AP-XPS, given that E-TEM, coupled with EELS, can also provide chemical information. EELS in E-TEM offers spatially resolved chemical insights, such as local oxidation states and bonding environments, with atomic-scale resolution. However, its utility is constrained by two critical factors. First, EELS is subject to operando limitations: it requires electron-transparent samples (typically $<\sim$100 nm in thickness) and performs more effectively at lower pressures (around 10^{-5} to 10^{-3} mbar). At higher pressures, the quality of spectra deteriorates due to increased electron scattering in the gas phase. This limitation makes EELS less suitable for studying realistic catalytic environments, which operate under near-ambient pressures and involve thicker or polycrystalline materials. Second, although EELS is highly effective for detecting light elements such as O and C under standard TEM conditions, its application in E-TEM is often constrained by the presence of gas, elevated temperatures, and potential sample drift—all of which can reduce the signal-to-noise ratio and spectral resolution. Moreover, in relatively thick samples or heterogeneous systems, the increased electron penetration depth results in a bulk-averaged signal that can obscure subtle surface changes and low-abundance species,[80,81] which are critical for understanding catalytic reactions.

In contrast, AP-XPS provides distinct advantages. It provides surface-specific, quantitative chemical information by operating at near-ambient pressure (up to 10 mbar), enabling the direct observation of adsorbates, oxidation states, and reaction intermediates under working conditions. Additionally, AP-XPS has statistical relevance, as it averages over μm-mm areas and captures ensemble-averaged chemical states that are representative of

practical catalysts (e.g., powders or polycrystalline films). This capability is essential for understanding the behavior of catalytic materials in realistic environments. Although AP-XPS exhibits lower elemental selectivity compared to techniques such as EELS, this limitation can also serve as an advantage in complex catalytic environments. By being less sensitive to trace elements, AP-XPS more selectively probes the dominant chemical states of key surface species, minimizing interference from minor or background signals. This facilitates clearer interpretation of redox processes and adsorption behaviors of the main active components under realistic reaction conditions.

The integration of E-TEM/EELS and AP-XPS creates a synergistic approach. While E-TEM/EELS excels at resolving local structural dynamics, it may miss important surface-specific chemistry. AP-XPS complements this gap by correlating global surface chemistry, such as adsorbate coverage and oxidation-state shifts, with catalytic activity. For example, in the water-gas shift reaction (WGSR) over Pt/CeO_2 catalysts, E-TEM reveals the dynamic restructuring of Pt NPs, while AP-XPS detects transient CO adsorption and $Pt^0/Pt^{\delta+}$ redox cycling[82]. These data, which are inaccessible to EELS due to its vacuum limitations and bulk probing nature, highlight the complementary strengths of both techniques.

Thus, the integration of E-TEM and AP-XPS is not redundant, but rather complementary. It bridges atomic-scale structural dynamics with surface chemistry under realistic conditions, offering multidimensional insights into chemical transformations and structural evolution. This combined approach overcomes the limitations of each individual technique, providing a comprehensive framework for investigating complex reaction mechanisms. Representative case studies, detailed in Table 1, demonstrate how integrating these techniques advances the understanding of heterogeneous catalytic systems.

Table 1: Recent examples of integrated E-TEM and AP-XPS studies on heterogeneous catalysts, highlighting the synergistic use of both techniques to probe structural and chemical dynamics.

Catalysts	Gas & Pressure	Temperature	Ref
Pt/CeO_2	E-TEM: O_2, 0.53 mbar; H_2, 0.53 mbar; CO, 0.13 mbar; H_2O vapor, 0.27 mbar AP-XPS: O_2, 0.53 mbar; H_2, 0.53 mbar; CO, 0.47 mbar; H_2O vapor, 0.93 mbar	400°C, 300°C	82
Pt/TiO_2	E-TEM: H_2, 1 bar; O_2, 1 bar AP-XPS: H_2, 0.15 mbar; O_2, 1 mbar	600 °C	54
Pt	E-TEM: UHV; air plasma AP-XPS: CO, 10 mbar; H_2, 0.5 mbar; H_2, O_2 plasma	127 °C, 227 °C RT, 100 °C	83

Ir NPs	E-TEM: UHV; H_2, 0.5 mbar	RT— 800°C	84
	AP-XPS: UHV	RT— 570°C	
$Cu_{50}Au_{50}$ NPs	E-TEM & AP-XPS: O_2, 1.33×10^{-3} mbar	200°C	25
CuO	E-TEM: H_2, 5×10^{-3} mbar	300 °C	50
	AP-XPS: O_2, 1.33 mbar; H_2, 5.3×10^{-3} mbar	350 °C, 300 °C	
Al	E-TEM: H_2O vapor, 4.67×10^{-5}—4.67×10^{-4} mbar	RT	85
	AP-XPS: H_2O vapor, 1.33×10^{-5} mbar		
Ti–Cu	ETEM: H_2, O_2, 1 bar	400 °C, 250 °C	86
	AP-XPS: H_2, O_2, 1 mbar		
Ni/γ–Mo_2N	E-TEM: H_2/N_2 = 3:1, 0.02 mbar	400 °C—520 °C	87
	AP-XPS: H_2/N_2 = 3:1, 0.053 mbar	300 °C—520 °C	
NiCu	E-TEM & AP-XPS: H_2, 1.33 mbar; ethanol, 0.27 mbar	350 °C, 250 °C	88
Cu-Au	E-TEM: H_2, 1.33×10^{-3} mbar	600 °C	89
	AP-XPS: H_2, 0.013 mbar		
Pt-CeO_2	E-TEM: H_2O:CO = 2:1, 0.73 mbar	200 °C	90
	AP-XPS: H_2O:CO = 2.3:1, 0.043 mbar	RT—300 °C	
Pd NPs	E-TEM: CH_4, 36.7 mbar; O_2, 16.7 mbar; He,126.6 mbar	350 °C, 550 °C	91
	AP-XPS: O_2, 1mbar; CH_4/O_2 = 4.5:1, 1.3 mbar		

A representative example of this combined approach is the study of Pt/CeO_2 catalysts during WGSR, where E-TEM and AP-XPS were integrated to elucidate the dynamic evolution of active sites.[82] Figure 2a-i illustrates the structural dynamics of Pt species supported on CeO_2 with different morphologies (rod, cube, and octahedron) using E-TEM. During O_2 and H_2 pretreatment, Pt atoms were highly dispersed and exhibited significant surface mobility. Under WGSR conditions (CO + H_2O at 300 °C), Pt gradually aggregated into small metallic clusters. This restructuring correlated with the formation of surface oxygen vacancies (V_O), suggesting that Pt atoms preferentially migrate and coalesce near vacancy-rich regions, leading to a reconfiguration of the metal–oxide interface. These observations highlight the intrinsically dynamic nature of the active sites and the structural adaptability of the interface under reaction conditions. Complementing the E-TEM observations, AP-XPS provided detailed insights into the changes in the oxidation states of Pt species during the WGSR. As shown in Figure 2j-o, after O_2 pretreatment, Pt was primarily present in oxidized forms (Pt^{4+} and Pt^{2+}), with a minor fraction as metallic Pt^0. Subsequent H_2 pretreatment partially reduced the oxidized Pt species to metallic Pt^0. Under WGSR conditions, metallic Pt^0 became the predominant species across all catalysts, while the rod-shaped Pt/CeO_2 catalyst retained the highest proportion of $Pt^{\delta+}$. These dynamic measurements on surface chemistry further emphasize the essential role of metal-support

interactions in stabilizing intermediate oxidation states and promoting catalytic activity. Taken together, E-TEM and AP-XPS jointly captured the complete dynamic evolution of the Pt/CeO_2 interface. This structure-driven, electronically coupled mechanism not only clarifies the nature of active sites under operando conditions but also underscores the indispensable role of integrated in situ techniques in unraveling the complexities of catalyst behavior at the atomic scale.

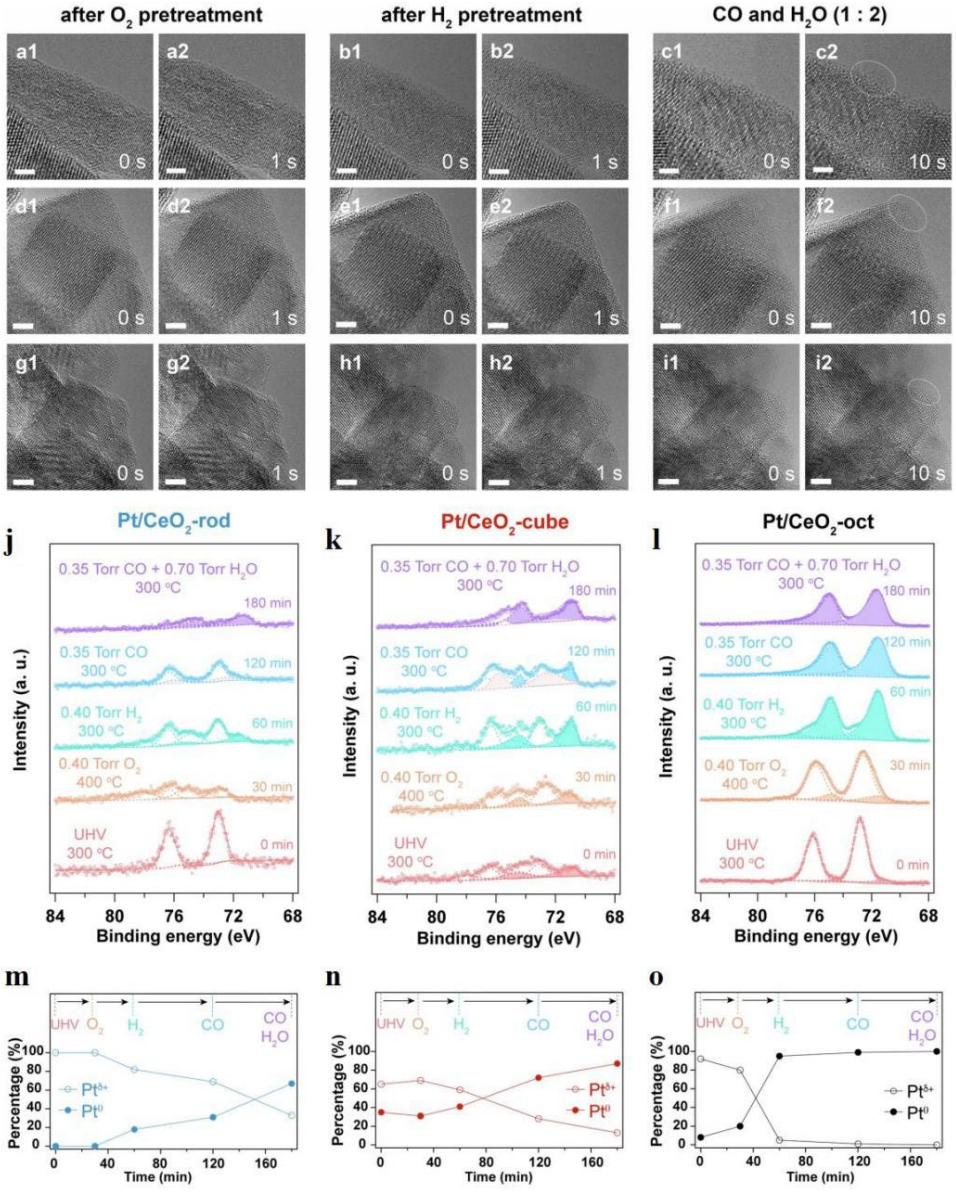

Figure 2. Operando correlation of Pt/CeO_2 structural dynamics and oxidation state evolution during WGSR. (a-i) Time-lapse E-TEM imaging of Pt/CeO_2 catalysts with distinct morphologies (rod: a–c; cube: d–f; octahedron: g–i). Snapshots were taken after O_2 pretreatment (400°C, 0.53 mbar, 30 min), H_2 pretreatment (300°C, 0.53 mbar, 30 min), and under WGSR conditions with CO (0.13 mbar) and H_2O (0.27 mbar) at 300°C. The images reveal the fluxional nature of Pt atoms, with dispersed species forming small clusters under reaction conditions. Scale bars, 2 nm. (j-o) AP-XPS analysis of Pt oxidation states during WGSR. (j–l) Pt 4f spectra of Pt/CeO_2-rod, Pt/CeO_2-cube, and Pt/CeO_2-oct catalysts collected under various conditions: UHV at 400°C, O_2 pretreatment (0.53 mbar, 400°C, 30

min), H_2 pretreatment (0.53 mbar, 300°C, 30 min), and WGSR conditions with CO (0.47 mbar) and H_2O (0.93 mbar) at 300°C. The pink solid peaks represent CO adsorption on metallic Pt^0 in the presence of CO and H_2O. (m–o) Fraction of Pt^0 and $Pt^{\delta+}$ species derived from peak areas under different conditions for the three catalysts. Solid circles represent Pt^0, while open circles represent $Pt^{\delta+}$. Adapted from ref 82. *Copyright 2024, Published by Nature Communications Materials.*

Similarly, in the study of Pt/TiO_2 catalysts under H_2 and O_2 atmospheres, Beck et al.[54] employed a combination of E-TEM and AP-XPS to uncover the dynamic behavior of the SMSI (Strong Metal-Support Interaction) phenomenon. Figures 3a-e depict the dynamic structural evolution of the Pt surface during the formation of SMSI. Under 1 bar H_2 at 600 °C, the Pt NPs gradually become coated with a low-contrast, amorphous overlayer (Figures 3a-b). Upon switching the atmosphere to O_2, the overlayer thickens, partial crystallization occurs, and lattice distortions emerge at the edges of the Pt particles (Figure 3c). Reintroduction of H_2 leads to significant thinning of the overlayer (Figure 3d), demonstrating the high reversibility of the SMSI state. Complementary to these structural changes, AP-XPS provides direct evidence of surface electronic modulation. Under H_2, the Pt $4f_{7/2}$ peak appears at 71.3 eV (Figure 3f), consistent with fully reduced metallic Pt. Upon exposure to O_2, the Pt signal decreases by approximately 50%, the binding energy shifts to 72.1 eV, and the peak broadens (Figure 3g), indicating electron transfer from Pt to the overlayer and the formation of interfacial Pt-O-Ti bonding. Reverting back to H_2 restores the Pt peak to its original intensity and binding energy (Figure 3h), in line with the overlayer thinning observed by E-TEM.

The strength of this study lies in its integrated use of real-space imaging and surface-sensitive spectroscopy. This dual approach not only confirms the causal link between TiO_x migration, overlayer formation, and Pt lattice distortion, but also reveals the directionality of charge transfer at the metal-oxide interface. By combining structural visualization with electronic state tracking, it overcomes the inherent limitations of single-technique analyses and enables a comprehensive, operando view of active site evolution. More broadly, this methodology provides critical experimental support for establishing a dynamic interface model. In SMSI systems, active site properties are not determined by a static encapsulation layer alone, but rather by the coordinated effects of a reversible TiO_x shell, localized lattice strain in the metal, and interfacial charge redistribution. This multifactor coupling serves as a conceptual foundation for next-generation catalyst design based on interface engineering principles.

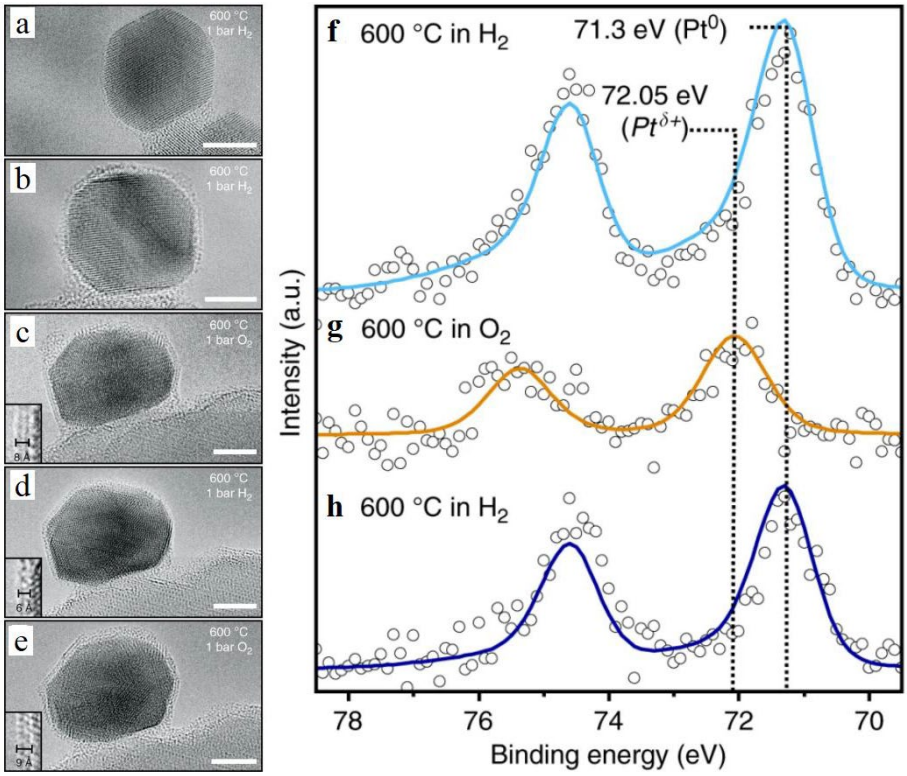

Figure 3. In-situ E-TEM and AP-XPS elucidating reversible structural dynamics and persistent chemical state changes of a Pt/TiO_2 catalyst during H_2 and O_2 cycling at 600 °C. (a-e) Time-resolved E-TEM imaging of a Pt nanoparticle on TiO_2 during alternating gas exposure: initial H_2 (1 bar, a-b), followed by O_2 (1 bar, c), H_2 (1 bar, d), and O_2 (1 bar, e) (scale bar: 5 nm). Insets in (c-e) show zoomed-in views of the overlayer structure observed. (k-m) AP-XPS Pt 4f spectra (650 eV photon energy) with corresponding peak fittings (Donjac-Sunjic for k, l, and Gaussian-Lorentian for m): metallic Pt^0 dominated after the first H_2 (0.15 mbar) exposure (k). Exposure to 1 mbar O_2 induced oxidation ($Pt^{\delta+}$) and a 50% intensity drop (l). Subsequent H_2 exposure (m) partially restored metallic Pt^0, but the total intensity remained low, indicating irreversible Pt redistribution or sintering. Adapted from ref 54. *Copyright 2020, The Author(s)*

Another notable example is the work by Liu et al.,[84] who combined E-TEM and AP-XPS to investigate the thermal evolution of Ir NPs on a carbon support (Ir/C), particularly focusing on the formation of carbon overcoats and their influence on catalyst stability and electronic structure. Figures 4a-p illustrate the real-time morphological transformation of Ir NPs under high vacuum heating. At around 550 °C, a thin carbon overlayer began to form on the Ir surface, which progressively graphitized and stabilized at 800 °C. This carbon shell effectively suppressed Ir NP sintering and migration, significantly enhancing the thermal stability of the catalyst at elevated temperatures. Meanwhile, in situ AP-XPS analysis (Figures 4q-s) provided complementary insights into the electronic state evolution of the Ir surface during the encapsulation process. In the initial material, the Ir 4f spectrum was dominated by a peak at 61.2 eV corresponding to Ir^{4+} species, along with a smaller contribution from metallic Ir^0 at 60.7 eV. The O 1s spectrum further confirmed the presence of surface Ir–O or Ir–OH species (530.3 eV), as well as surface oxygen associated with the

carbon support (531.9 eV). Upon heating to 200 °C, the Ir^{4+} peak decreased significantly and eventually disappeared, indicating the reduction of surface Ir oxides to metallic Ir. This reduction process was accompanied by a rise in the chamber pressure, suggesting desorption of adsorbed water and/or decomposition of IrOx species. As the temperature was further increased to 400-570 °C, the Ir 4f peak remained at the binding energy position associated with metallic Ir, but its intensity gradually declined. This trend is consistent with the thickening of the carbon overlayer observed in TEM, which attenuates the Ir signal due to increased surface coverage. Notably, the C 1s spectrum showed a marked increase in the 284.3 eV peak with rising temperature, indicating reorganization and graphitization of the carbon support surface. This trend was inversely correlated with the weakening Ir signal, suggesting enhanced attenuation of the Ir signal by the growing carbon overlayer, thereby supporting the formation of a stable encapsulation structure.

The strength of this study lies in the high complementarity between in situ TEM and AP-XPS. While TEM captured nanoscale structural transformations on the particle surface, such as overlayer formation, thickness evolution, and morphological changes, AP-XPS provided dynamic tracking of the elemental valence states, particularly offering key insights into the reduction of Ir from its oxidized state to metallic Ir, interfacial electron transfer behavior, and the restructuring of the carbon matrix. The combined use of in situ TEM and AP-XPS enables real-time monitoring of both the structural and electronic evolution of the active centers, revealing the stepwise formation of carbon overcoating as a stabilization mechanism. This integrated approach offers strong mechanistic support and strategic guidance for the rational design of thermally robust noble metal catalysts.

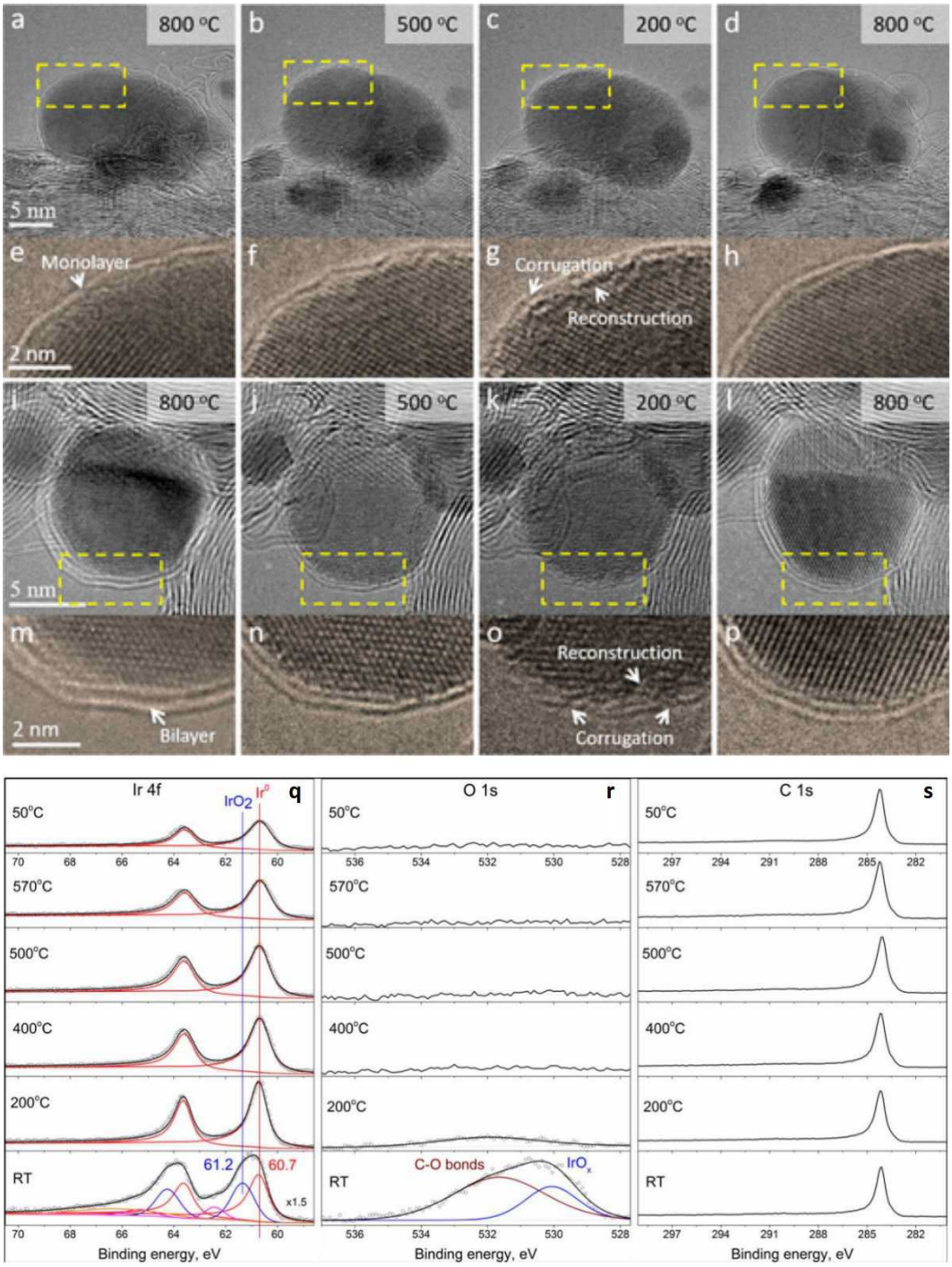

Figure 4: In-situ atomic-scale TEM and XPS observations of the structural and electnic evolution of Ir NPs on a carbon support during temperature cycling. (a-p) In situ TEM images showing changes in the overlayer and interfacial structure at temperatures of 800, 500, 200 ℃, and back to 800 ℃. (a−d) Monolayer carbon-covered Ir NP; (e−h) Enlarged images within the dotted rectangles in (a−d); (i−l) Bilayer carbon-covered Ir NP; (m−p) Enlarged images from the dotted rectangles in (i−l). (q-s) XPS spectra of (q) Ir 4f, (r) O 1s, and (s) C 1s for Ir/C at temperatures ranging from RT to 570 ℃ under UHV conditions. Adapted from ref 84. *Copyright 2023, American Chemical Society.*

These studies highlight the significant potential of integrating E-TEM and AP-XPS for investigating the structural dynamics and chemical transformations of heterogeneous

catalysts. The synergistic use of these techniques provides a more comprehensive understanding of the intricate interplay between structural evolution and surface chemical behavior under similar reaction conditions. Below, we highlight three studies from our own research, demonstrating how the complementary capabilities of these tools have been leveraged to explore the redox behavior of metals, alloys and oxides.

Wang et al.[25] employed a combination of in situ AP-XPS and E-TEM to investigate the oxygen-induced encapsulation of $Cu_{50}Au_{50}$ NPs supported on HOPG, revealing a representative case of carbon-based SMSI. As shown in Figures 5a-f, under conditions of 200 °C and increasing O_2 pressure, AP-XPS revealed distinct peaks in the C 1s (290.4 eV) and O 1s (532.3 eV) regions, indicating the progressive formation of surface graphitic oxides (O–C═O). These signals were significantly stronger for $Cu_{50}Au_{50}$/HOPG compared to Au/HOPG, suggesting that the alloy promoted the formation of a graphitic oxide layer encapsulating the surface. Concurrently, Cu 2p spectra revealed the development of Cu^{2+}-like states, distinct from typical CuO signatures, which were attributed to interface charge transfer between Cu atoms and O–C═O ligands, leading to a $3d^9L^{-2}$ final-state configuration. Depth profiling with variable photon energies further confirmed the presence of an ultrathin graphitic oxide overlayer on the $Cu_{50}Au_{50}$ NPs, where the Cu and Au signals were undetectable with low-energy photons but visible with high-energy excitation (~650 eV). This indicated that the overlayer thickness consisted of only a few carbon layers. These spectroscopic insights were complemented by real-space imaging via E-TEM under similar reaction conditions. Figures 5g-l show in-situ HRTEM images, revealing that the graphitic oxide shell initiated at the NP/HOPG contact corners and gradually spread over the entire NP surface, forming a 1–2 layer-thick encapsulation with an interlayer spacing of ~0.4 nm—larger than that of pristine graphite (0.33 nm)—indicating partial oxidation of the graphitic structure. Unlike traditional SMSI systems, which involve oxide supports and reversible encapsulation, this work introduces an encapsulation mechanism on carbon supports. It demonstrates how the combination of AP-XPS and E-TEM enables complementary, multiscale insight into structure–electronic–function relationships at the catalytic interface.

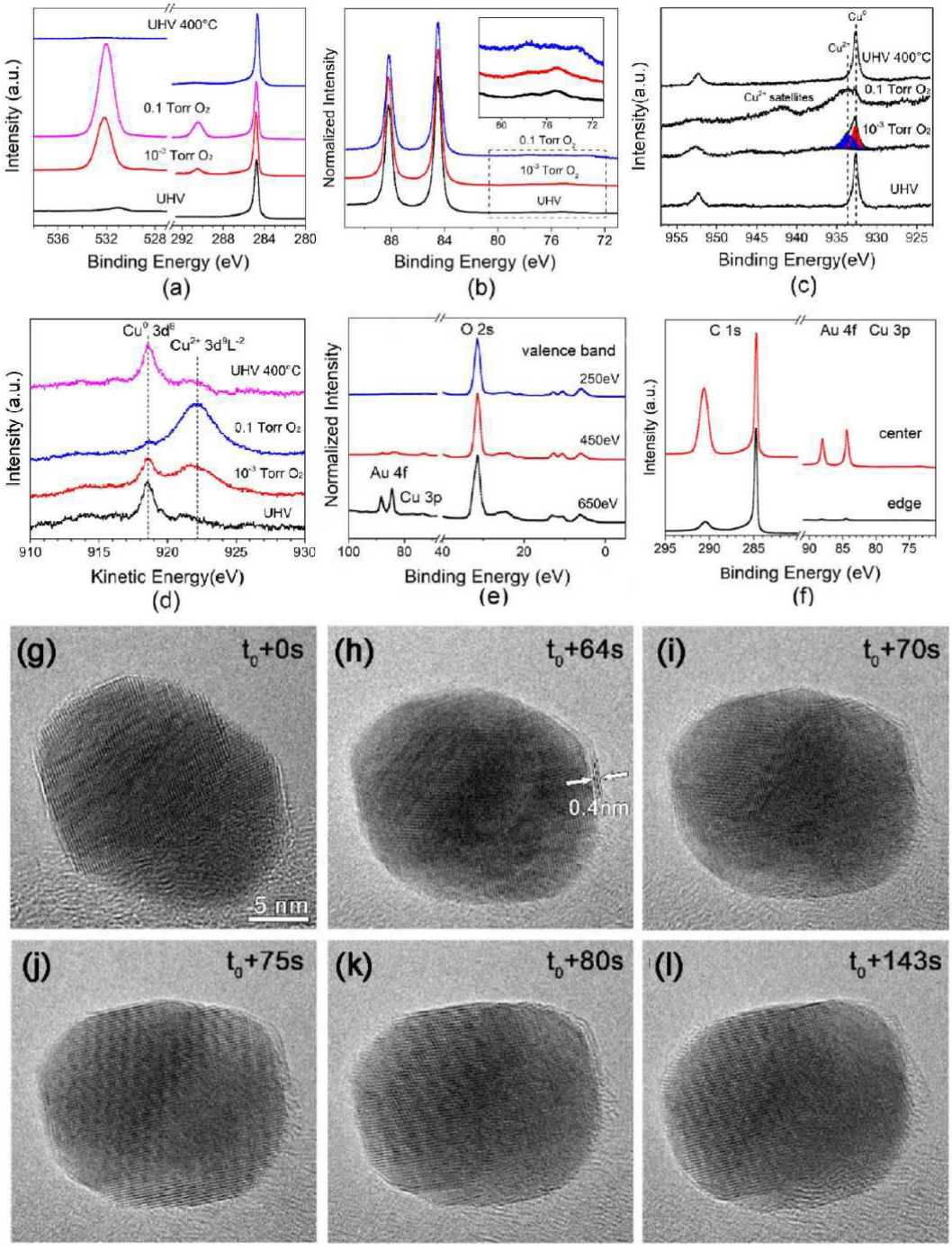

Figure 5. Chemical and structural dynamics of $Cu_{50}Au_{50}$NPs on HOPG under O_2 exposure. (a–d) Evolution of AP-XPS spectra at 200 °C showing the formation of a graphitic oxide layer. Key regions include O 1s, C 1s, Au 4f, Cu 3p, Cu 2p, and Cu LMM. The spectra in the top sections of (a, c, d) correspond to UHV annealing at 400 °C after O_2 dosing, revealing the decomposition of the graphitic oxide layer. The inset in (b) highlights the Cu 3p region, showing that the O_2 exposure did not fully form CuO, consistent with electron transfer to carbon and oxygen species under photon excitation. (e) Au 4f, Cu 3p, and O 2s spectra illustrating that the graphitic oxide is primarily localized at the uppermost surface layers measured with the photon energies of 250 eV, 450, and 600 eV, respectively (200 °C, 1.33×10^{-3} mbar O_2). (f) Comparative Au 4f and C 1s spectra obtained from the center (high density of $Cu_{50}Au_{50}$ NPs) and edge regions (no $Cu_{50}Au_{50}$ NPs) of the HOPG support, demonstrating

that the graphitic oxide formed predominantly on the $Cu_{50}Au_{50}$NPs. (g–l) Time-lapse HRTEM images illustrating the encapsulation of $Cu_{50}Au_{50}$ NPs during O_2 exposure (200 °C, 1.33×10^{-3} mbar O_2). Adapted from ref 25. *Copyright 2024, American Chemical Society.*

Another example of this combined methodology is the study by Sun et al.,[50] which investigated H_2-induced structural oscillations in CuO, leveraging in situ capabilities of E-TEM and AP-XPS to elucidate the dynamic interplay between surface reactions and subsurface structural changes. Figures 6a–d present E-TEM imaging that vividly captured the dynamic superlattice oscillations occurring within the ~3 nm subsurface region of CuO under H_2 atmosphere. These oscillations reflected the periodic ordering and disordering of oxygen vacancies, confined to a shallow "active layer" near the surface (confirmed by FFT in Figures 6e–l). The absence of deeper lattice involvement suggests that the reaction-induced nonstoichiometric modulation was spatially localized, revealing how surface reactions—through vacancy formation and migration—can structurally perturb the near-surface lattice without altering the bulk. Complementary insights were provided by AP-XPS analysis in Figure 6g. The O 1s spectrum evolves from a single lattice oxygen peak at 529.5 eV to a broadened profile with a shoulder at 530.6 eV, indicating the formation and accumulation of surface hydroxyl (OH) species. This electronic transition reflected H_2-induced activation of lattice oxygen and subsequent vacancy generation. Notably, the emergence of the OH-related shoulder closely paralleled the structural oscillations observed by E-TEM, suggesting that surface chemistry evolution dynamically regulated subsurface structural responses.

This study demonstrated the strong complementarity between in situ AP-XPS and E-TEM: E-TEM offers atomic-scale resolution of vacancy ordering and disordering by real-time visualization of structural oscillations, while AP-XPS reveals the associated sequence of electronic changes—OH formation, H_2O desorption, and vacancy generation—through spectral broadening and the emergence of identifiable intermediates. Together, they uncovered a dynamic surface-subsurface coupling mechanism linking vacancy generation at the oxide surface, structural response in the subsurface, and reaction intermediate (OH) modulation, highlighting the power of multimodal operando characterization in advancing our understanding of heterogeneous catalysis.

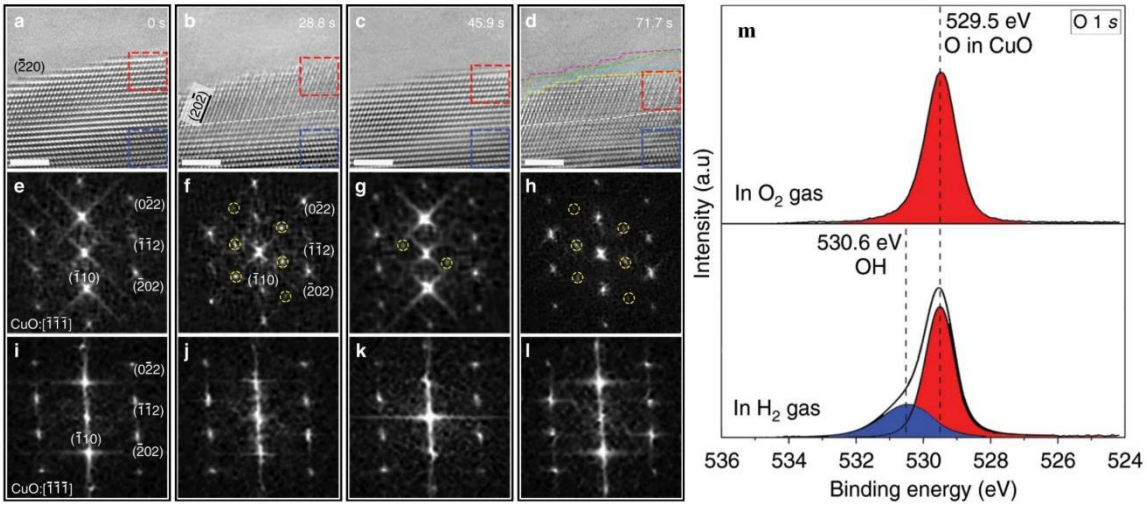

Figure 6. E-TEM and AP-XPS monitoring of CuO reduction in H_2. (a-d) Time-resolved HRTEM images of the CuO lattice during exposure to a continuous flow of H_2 gas at 300 °C and 5×10^{-3} mbar H_2. The pink, green, arctic, and yellow dashed lines in (d) trace the position and configuration of the outer surface at 0 s, 28.9 s, 45.9 s, and 71.7 s, respectively, illustrating the oxide decay via receding motion of atomic steps at the outer surface. The white dashed lines in (b, d) mark the boundary between the superlattice region and the deeper, unaffected region. (e–h) Diffractograms from the subsurface region (red dashed box in HRTEM images), showing the cyclic reoccurrence of superlattice diffraction spots indicated by yellow dashed circles. (i–l) Diffractograms from the deeper region (blue dashed box in HRTEM images), revealing that the deeper regions of the CuO lattice remained unaffected throughout the process. Scale bar: 2 nm (a–d). (m) Photoelectron spectra of O 1s obtained from the CuO surface at 1.33 mbar O_2 and 350 °C (upper panel), and subsequent exposure to 5.3×10^{-3} mbar H_2 at 300 °C (lower panel). H_2 exposure induced broadening of the O 1s spectrum toward higher binding energy, with the major peak corresponding to lattice oxygen in CuO (red) and the shoulder peak ascribed to surface OH groups (blue). Adapted from ref 50. *Copyright 2020, The Author(s)*

Beyond catalysis reactions, the combination of E-TEM and AP-XPS proves invaluable for studying other gas-surface reactions such as meal oxidation and passivation,[85,92,93] which can contribute to catalyst degradation. For example, recent work by Chen et al.[85] investigated the atomic-scale passivation dynamics of Al surfaces in H_2O vapor, offering new insights into its structural evolution and functional properties. Their results showed that H_2O vapor induces the formation of a bilayer oxide structure: an outer crystalline $Al(OH)_3$ layer and an inner amorphous Al_2O_3 layer, as illustrated in Figure 7a-i. In situ high-resolution E-TEM imaging revealed that upon initial contact of H_2O vapor, the clean Al surface forms a crystalline $Al(OH)_3$ layer approximately 5.0 Å thick. Over time, inward diffusion of oxygen atoms drives the growth and thickening of the inner amorphous Al_2O_3 layer. This bilayer structure exhibits a self-limiting growth behavior, consistent with the Cabrera-Mott oxidation model.

The in-situ E-TEM observations were further corroborated by AP-XPS, which provided detailed insights into the chemical composition and temporal evolution of the Al_2O_3 and

$Al(OH)_3$ layers. Complementary insights were provided by in situ AP-XPS and residual gas analysis (RGA) in Figures 7j-l, which elucidated the chemical transformations and gas-phase reaction pathways underlying the observed structural changes. The O 1s spectra showed a rapid increase and subsequent saturation of the OH peak at 533.8 eV, while the O peak at 532.1 eV continued to grow, mirroring the sequential formation of $Al(OH)_3$ followed by Al_2O_3 observed via E-TEM. Simultaneously, RGA monitoring revealed a transient release of H_2 gas, confirming that H_2O dissociation occurred on the Al surface, followed by H–O recombination and H_2 evolution—a characteristic passivation reaction route. Importantly, the bilayer film formation observed in E-TEM was in excellent agreement with the time-resolved electronic and gas-phase signals captured in Figures 7j-l, establishing a comprehensive temporal and mechanistic correlation. AP-XPS quantified the transition between OH and O surface species, while RGA provided kinetic evidence of H_2 evolution, which underlined the saturation of oxide film thickness seen in E-TEM.

This work highlights the powerful synergy of E-TEM and AP-XPS in probing heterogeneous interface reactions. By combining atomic-scale imaging, surface chemistry, and gas evolution analysis, the study bridges structural, electronic, and kinetic dimensions. This integrative approach enables a full-spectrum understanding of metal oxidation and passivation processes, offering key mechanistic insights for corrosion resistance, interfacial design, and surface reaction engineering.

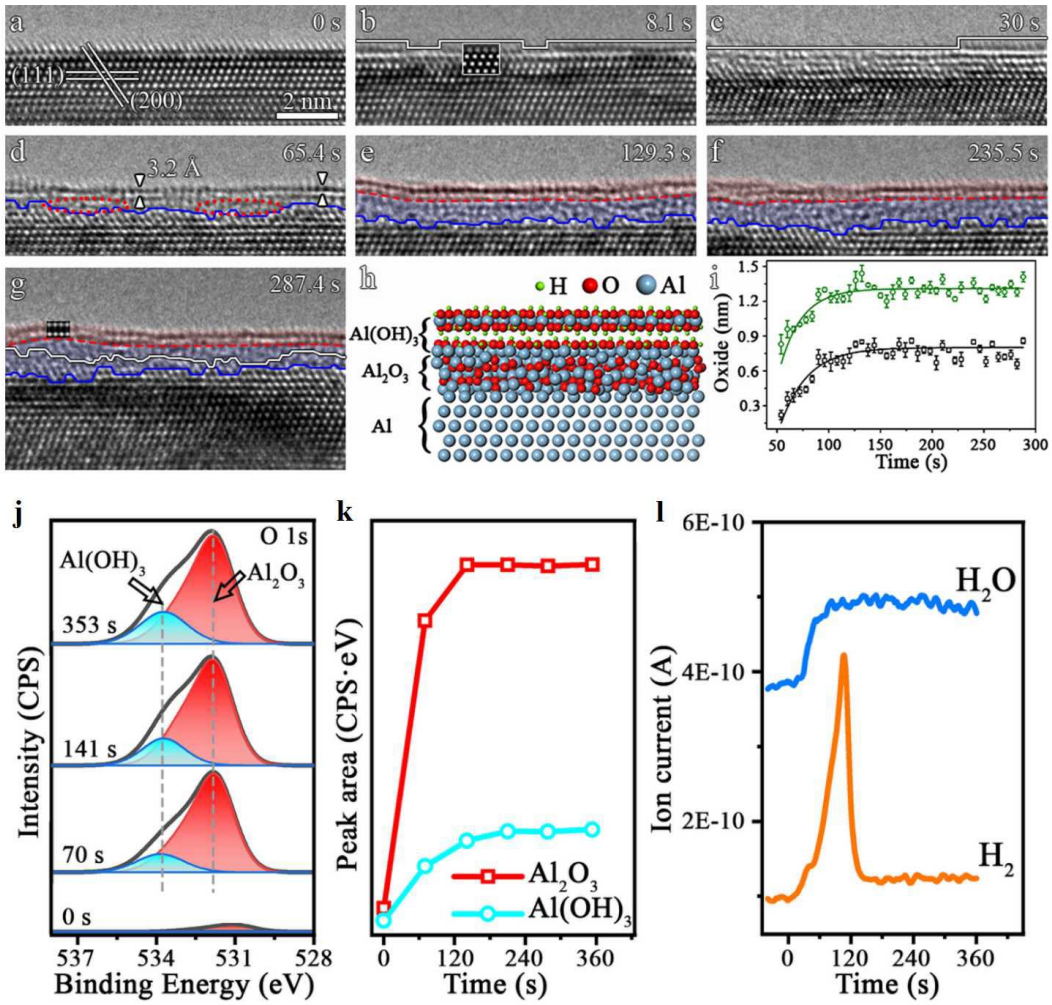

Figure 7. Coordinated E-TEM and AP-XPS monitoring of surface passivation of Al(111) by H_2O vapor, demonstrating the formation of an $Al(OH)_3/Al_2O_3$ bilayer. (a-g) Time-sequence HRTEM images showing the $Al(OH)_3/Al_2O_3$ bilayer growth on Al(111) at 25 °C and 4.67×10^{-5} mbar H_2O. White lines highlight regions with weakened lattice contrast due to H_2O-induced Al extraction from the outermost Al(111) layer. Red dashed lines and blue solid lines denote the $Al(OH)_3/Al_2O_3$ and Al_2O_3/Al(111) interfaces, respectively. The white line in (g) traces the Al_2O_3/Al(111) interface position from (d) at t=65.4 s. Insets in (b) and (g) are simulated HRTEM images of the Al lattice with surface vacancies and the $Al(OH)_3$ structure. (h) Schematic of the $Al(OH)_3/Al_2O_3$ bilayer structure. (i) Time-dependent thickness of the $Al(OH)_3/Al_2O_3$ bilayer (green) and Al_2O_3/Al(111) interface displacement (black). The $Al(OH)_3$ layer reaches ~5.0 Å thickness after ~60 s, while the inner Al_2O_3 layer grows to a limiting thickness. Error bars show standard deviation uncertainties from multiple measurements. (j-l) AP-XPS and residual gas analyzer (RGA) measurements of passive oxide film formation on Al(111). (j) Time-resolved O 1s photoemission spectra and CPS during Al(111) exposure to 1.33×10^{-5} mbar H_2O at 25 °C. The faint peak at 0 s is attributed to residual oxygen from incomplete sputtering and annealing. (k) Time evolution of integrated intensities for Al_2O_3 and $Al(OH)_3$ components. (l) RGA measurements showing H_2O consumption (blue) and H_2 production (orange). Adapted from ref 85. *Copyright 2023, The Authors, some rights reserved*

The integration of E-TEM and AP-XPS provides a robust toolkit for studying structural and chemical evolution of heterogeneous catalysts, as well as the underlying reaction mechanisms. These complementary techniques offer real-time, dynamic insights into catalyst behavior under realistic reaction conditions: E-TEM enables atomic-scale visualization of catalyst structures, capturing phenomena such as NP reconstruction, dynamic growth of surface oxide layers, and adaptation at metal-support interfaces.[94] On the other hand, AP-XPS probes ensemble-level changes in surface chemistry, adsorption and activation of reactants, and the formation of reaction intermediates, offering a detailed view of the chemical evolution of catalysts.[59] By combining these methods, researchers can bridge macroscopic catalytic performance with atomic-level mechanisms. Enabling a comprehensive understanding of structure-property relationships. For instance, the integrated use of E-TEM and AP-XPS has proven instrumental in studying dynamic processes like SMSI, monitoring the chemical states of intermediates, and elucidating their roles in key reactions, such as CO oxidation and the water-gas shift reaction.[25,84] These studies have provided critical experimental evidence for understanding the mechanisms governing heterogeneous catalysis.

Furthermore, Karagoz et al.[95] developed a custom-designed microheater holder to integrate MEMS microheater chips, originally utilized for E-TEM experiments, into AP-XPS systems. This innovative adaptation demonstrated the successful incorporation of MEMS microheaters into AP-XPS, enabling rapid heating, time-resolved measurements, and localized gas quantification. The results confirmed the feasibility of employing MEMS heaters for real-time investigations of catalytic processes under near-industrial conditions. This work paves the way for multimodal characterization by combining AP-XPS and E-TEM to achieve a comprehensive understanding of heterogeneous catalysis. Future advancements, such as incorporating electron-transparent membranes for high-pressure studies, are expected to further expand the capabilities of this approach.

However, both techniques face challenges that require further advancements in methodology and experimental design. Despite the widespread use of E-TEM in heterogeneous catalysis research,[96] the high-brightness, high-stability electron beams required for high-resolution imaging inevitably interact with catalysts,[97] gases,[98] and even window materials,[99] leading to electron beam effects such as breakdown damage, electrostatic charging, and ionization damage (radiolysis).[19,22] Mitigation strategies include reducing electron beam energy below critical thresholds or lowering the dose rate.[28,100] For example, integrated differential phase contrast scanning transmission electron microscopy (iDPC-STEM) significantly reduces the dose rate. Using this technique, Shen and Wang et al. [101] achieved atomic-level imaging of small molecules (e.g., pyridine and thiophene) within ZSM-5 channels at room temperature, overcoming the limitations of single-molecule atomic-scale imaging. Moreover, comparisons between non-irradiated and continuously irradiated samples enable evaluation of beam-induced damage. Additionally, the incorporation of direct electron detectors allows for ultra-fast imaging with dramatically reduced electron dose rates during in-situ TEM imaging, further minimizing beam-induced artifacts.

Similarly, AP-XPS, despite its capability to perform in situ studies of heterogeneous catalytic systems under reaction conditions—including monitoring chemical changes and formation of intermediates[58,102,103]—faces its own set of limitations. The high-energy X-rays used in AP-XPS can cause radiation damage to samples and induce undesired activation or dissociation of gas-phase reactants. Additionally, the high precision required for sample positioning and stability during analysis imposes significant demands on both the sample preparation and the instrumentation,[123] limiting its efficiency for certain types of experiments.

Another significant challenge is that both E-TEM and AP-XPS are constrained by their operational pressure limits, which are far below those of industrial catalytic processes (often exceeding hundreds of bars). Future developments should focus on designing analytical tools capable of stable operation under higher pressures. One promising strategy involves the use of graphene membrane-based flow reaction cells, which offer a potential solution to the limitations imposed by high-pressure differentials. These cells are specifically designed for AP-XPS and can sustain gas environments up to 1 bar on the reaction side while maintaining ultrahigh vacuum on the detection side, thereby enabling surface-sensitive chemical analysis under realistic catalytic conditions.[104] For example, the graphene-encapsulated microcell developed by Tao et al. facilitates surface XPS measurements of catalysts under flowing gas conditions using a conventional high-vacuum XPS system. This platform is particularly well-suited for investigating the evolution of valence states in powder catalysts under industrially relevant environments.[105] Furthermore, integrating E-TEM and AP-XPS with other in situ techniques, such as X-ray absorption spectroscopy (XAS) and infrared reflection absorption spectroscopy (IRRAS), is crucial for achieving a more comprehensive, multiscale understanding of catalytic processes.[106-108] Multimodal approaches can enable the characterization of catalysts across multiple scales, from surface to bulk and from electronic structure to dynamic behavior, providing a holistic view of complex catalytic systems. As an example, Nguyen et al. developed a static liquid cell that enabled XPS analysis of silver nanoparticles in a liquid environment, complemented by SEM imaging to confirm particle distribution. This work offers a valuable technical reference for investigating the electronic structure at liquid-solid interfaces.[109]

In conclusion, the combination of E-TEM and AP-XPS offers a powerful and complementary approach for investigating heterogeneous catalysis. As these techniques continue to evolve, advancements in higher-resolution imaging, operation under more industrially relevant pressure conditions, and integration with other complementary in situ methods will further expand their capabilities and applicability. These developments will be instrumental in elucidating complex reaction mechanisms and guiding the rational design of more efficient and durable catalysts for a wide range of applications. By bridging the gap between fundamental research and practical catalyst development, E-TEM and AP-XPS will play a crucial role in shaping the future of catalysis science and technology.

Acknowledgments: This work was supported by the U.S. National Science Foundation Under Grant No. DMR 2303712.

REFERENCES

(1) Ge, S.; Fan, W.; Tang, X.; Cui, Y.; Wang, D.; Gong, X.-Q.; Dai, S.; Lou, Y.; Tang, J.; Guo, Y. Revealing the Size Effect of Ceria Nanocube-Supported Platinum Nanoparticles in Complete Propane Oxidation. *ACS Catal.* **2024**, *14* (4), 2532-2544. https://doi.org/10.1021/acscatal.3c06139.

(2) Taulo, G. T.; Shaalan, N. M.; Mohamed, G. G.; Ayad, M. M.; Abd El-Moneim, A. Inkjet Printing of SnO_2 Nanoparticles with Exposed High-Energy Facets for CO Gas Sensing. *Ceram. Int.* **2024**, *50* (11), 18638-18646. https://doi.org/10.1016/j.ceramint.2024.02.352.

(3) Wang, G.; Ke, X.; Sui, M. Advanced TEM Characterization for Single-Atom Catalysts: from ex-situ Towards in-situ. *Chem. Res. Chin. Univ.* **2022**, *38* (5), 1172-1184. https://doi.org/10.1007/s40242-022-2245-0.

(4) Tan, H. L.; Abdi, F. F.; Ng, Y. H. Heterogeneous Photocatalysts: An Overview of Classic and Modern Approaches for Optical, Electronic, and Charge Dynamics Evaluation. *Chem. Soc. Rev.* **2019**, *48* (5), 1255-1271. DOI: 10.1039/C8CS00882E.

(5) Liu, L.; Corma, A. Metal Catalysts for Heterogeneous Catalysis: From Single Atoms to Nanoclusters and Nanoparticles. *Chem. Rev.* **2018**, *118* (10), 4981-5079. https://doi.org/10.1021/acs.chemrev.7b00776.

(6) Li, Z.; Ji, S.; Liu, Y.; Cao, X.; Tian, S.; Chen, Y.; Niu, Z.; Li, Y. Well-Defined Materials for Heterogeneous Catalysis: From Nanoparticles to Isolated Single-Atom Sites. *Chem. Rev.* **2019**, *120* (2), 623-682. https://doi.org/10.1021/acs.chemrev.9b00311.

(7) Low, J.; Yu, J.; Jaroniec, M.; Wageh, S.; Al-Ghamdi, A. A. Heterojunction Photocatalysts. *Adv. Mater.* **2017**, *29* (20), 1601694. https://doi.org/10.1002/adma.201601694.

(8) Seh, Z. W.; Kibsgaard, J.; Dickens, C. F.; Chorkendorff, I.; Nørskov, J. K.; Jaramillo, T. F. Combining Theory and Experiment in Electrocatalysis: Insights into Materials Design. *Science* **2017**, *355* (6321), eaad4998. DOI: 10.1126/science.aad4998.

(9) Saha, D.; Yu, H.-J.; Wang, J.; Prateek; Chen, X.; Tang, C.; Senger, C.; Pagaduan, J. N.; Katsumata, R.; Carter, K. R. Mesoporous Single Atom-Cluster Fe–N/C Oxygen Evolution Electrocatalysts Synthesized with Bottlebrush Block Copolymer-Templated Rapid Thermal Annealing. *ACS Appl. Mater. Interfaces* **2024**, *16* (11), 13729-13744. https://doi.org/10.1021/acsami.3c18693.

(10) Gao, W.; Hood, Z. D.; Chi, M. Interfaces in Heterogeneous Catalysts: Advancing Mechanistic Understanding through Atomic-Scale Measurements. *Acc. Chem. Res.* **2017**, *50* (4), 787-795. https://doi.org/10.1021/acs.accounts.6b00596.

(11) Wu, D.; Zhu, Y.; Shan, W.; Wang, J.; Liu, Q.; Zhou, G. Revealing an Intermediate Cu–O/OH Superstructure on Cu (110). *J. Phys. Chem. Lett.* **2022**, *13* (10), 2396-2403. https://doi.org/10.1021/acs.jpclett.1c04145.

(12) Xiao, L.; Qi, L.; Sun, J.; Husile, A.; Zhang, S.; Wang, Z.; Guan, J. Structural Regulation of Covalent Organic Frameworks for Advanced Electrocatalysis. *Nano Energy* **2024**, *120*, 109155. https://doi.org/10.1016/j.nanoen.2023.109155.

(13) Groppo, E.; Rojas-Buzo, S.; Bordiga, S. The Role of in Situ/Operando Ir Spectroscopy in Unraveling Adsorbate-Induced Structural Changes in Heterogeneous Catalysis. *Chem. Rev.* **2023**, *123* (21), 12135-12169. https://doi.org/10.1021/acs.chemrev.3c00372.

(14) Sun, Y.-L.; Deng, Y.-L.; Chen, H.-N.; Yang, X.-T.; Lin, X.-M.; Li, J.-F. Design Strategies and in Situ Infrared, Raman, and X-Ray Absorption Spectroscopy Techniques Insight into the Electrocatalysts of Hydrogen Energy System. *Small Struct.* **2023**, *4* (6), 2200201. https://doi.org/10.1002/sstr.202200201.
(15) Zhang, X.; Zhang, M.; Deng, Y.; Xu, M.; Artiglia, L.; Wen, W.; Gao, R.; Chen, B.; Yao, S.; Zhang, X. A Stable Low-Temperature H_2-Production Catalyst by Crowding Pt on α-MoC. *Nature* **2021**, *589* (7842), 396-401. https://doi.org/10.1038/s41586-020-03130-6.
(16) Xie, Y.; Sun, Y.; Tao, H.; Wang, X.; Wu, J.; Ma, K.; Wang, L.; Kang, Z.; Zhang, Y. In Situ Investigation on Life-Time Dynamic Structure–Performance Correlation toward Electrocatalyst Service Behavior in Water Splitting. *Adv. Funct. Mater.* **2022**, *32* (18), 2111777. https://doi.org/10.1002/adfm.202111777.
(17) Zhou, S.; Yang, Y.; Yin, P.; Ren, Z.; Wang, L.; Wei, M. Metal–Support Synergistic Catalysis in Pt/MoO_{3-X} Nanorods toward Ammonia Borane Hydrolysis with Efficient Hydrogen Generation. *ACS Appl. Mater. Interfaces* **2022**, *14* (4), 5275-5286. https://doi.org/10.1021/acsami.1c20736.
(18) Dupraz, M.; Li, N.; Carnis, J.; Wu, L.; Labat, S.; Chatelier, C.; van de Poll, R.; Hofmann, J. P.; Almog, E.; Leake, S. J. Imaging the Facet Surface Strain State of Supported Multi-Faceted Pt Nanoparticles during Reaction. *Nat. Commun.* **2022**, *13* (1), 3003. https://doi.org/10.1038/s41467-022-30592-1.
(19) Qu, J.; Sui, M.; Li, R. Recent Advances in in-Situ Transmission Electron Microscopy Techniques for Heterogeneous Catalysis. *IScience* **2023**, *26* (7), 107072. DOI: 10.1016/j.isci.2023.107072.
(20) Dai, J.; Sun, Y.; Liu, Z.; Zhang, Y.; Duan, S.; Wang, R. Using in Situ Transmission Electron Microscopy to Study Strong Metal-Support Interactions in Heterogeneous Catalysis. *Angew. Chem.* **2024**, *136* (42), e202409673. https://doi.org/10.1002/ange.202409673.
(21) Tao, F. Development of New Methods of Studying Catalyst and Materials Surfaces with Ambient Pressure Photoelectron Spectroscopy. *Acc. Chem. Res.* **2025**, *58* (1), 11-23. https://doi.org/10.1021/acs.accounts.4c00508.
(22) Hwang, S.; Chen, X.; Zhou, G.; Su, D. In Situ Transmission Electron Microscopy on Energy-Related Catalysis. *Adv. Energy Mater.* **2020**, *10* (11), 1902105. https://doi.org/10.1002/aenm.201902105.
(23) Tang, M.; Yuan, W.; Ou, Y.; Li, G.; You, R.; Li, S.; Yang, H.; Zhang, Z.; Wang, Y. Recent Progresses on Structural Reconstruction of Nanosized Metal Catalysts Via Controlled-Atmosphere Transmission Electron Microscopy: A Review. *ACS Catal.* **2020**, *10* (24), 14419-14450. https://doi.org/10.1021/acscatal.0c03335.
(24) Deng, K.; Chen, X.; Moncada, J.; Salvatore, K. L.; Rui, N.; Xu, W.; Xiang, S.; Marinkovic, N.; Frenkel, A. I.; Zhou, G. Observing Chemical and Morphological Changes in a Cu@TiO_X Core@Shell Catalyst: Impact of Reversible Metal-Oxide Interactions on CO_2 Activation and Hydrogenation. *ACS Catal.* **2024**, *14* (15), 11832-11844. https://doi.org/10.1021/acscatal.4c02694.
(25) Wang, J.; Chen, X.; Li, C.; Zhu, Y.; Li, J.; Shan, S.; Hunt, A.; Waluyo, I.; Boscoboinik, J. A.; Zhong, C.-J. Tuning Strong Metal–Support Interactions Via Synergistic Alloying. *ACS Catal.* **2024**, *14* (8), 5662-5674. https://doi.org/10.1021/acscatal.3c06171.

(26) Mehar, V.; Kim, J.; Hunt, A.; Waluyo, I.; Rodriguez, J. A. AP-XPS Study of the Reaction of O_2 and CO_2 with Zn–Au (111) Surface Alloys: Activation of O–O/C–O Bonds and the Formation of ZnO. *J. Phys. Chem. C* **2024**, *128* (33), 13852-13863. https://doi.org/10.1021/acs.jpcc.4c03321.
(27) Zhao, S.; Yang, Y.; Tang, Z. Insight into Structural Evolution, Active Sites, and Stability of Heterogeneous Electrocatalysts. *Angew. Chem. Int. Ed.* **2022**, *61* (11), e202110186. https://doi.org/10.1002/anie.202110186.
(28) Zhang, F.; Liu, W. Recent Progress of Operando Transmission Electron Microscopy in Heterogeneous Catalysis. *Microstructures* **2024**, *4* (3), 2024041. 10.20517/microstructures.2024.03.
(29) Boyes, E. D.; LaGrow, A. P.; Ward, M. R.; Mitchell, R. W.; Gai, P. L. Single Atom Dynamics in Chemical Reactions. *Acc. Chem. Res.* **2020**, *53* (2), 390-399. https://doi.org/10.1021/acs.accounts.9b00500.
(30) He, B.; Zhang, Y.; Liu, X.; Chen, L. In-Situ Transmission Electron Microscope Techniques for Heterogeneous Catalysis. *ChemCatChem* **2020**, *12* (7), 1853-1872. https://doi.org/10.1002/cctc.201902285.
(31) Cheng, H. W.; Wang, S.; Chen, G.; Liu, Z.; Caracciolo, D.; Madiou, M.; Shan, S.; Zhang, J.; He, H.; Che, R. Insights into Heterogeneous Catalysts under Reaction Conditions by in Situ/Operando Electron Microscopy. *Adv. Energy Mater.* **2022**, *12* (38), 2202097. https://doi.org/10.1002/aenm.202202097.
(32) Chao, H.-Y.; Venkatraman, K.; Moniri, S.; Jiang, Y.; Tang, X.; Dai, S.; Gao, W.; Miao, J.; Chi, M. In Situ and Emerging Transmission Electron Microscopy for Catalysis Research. *Chem. Rev.* **2023**, *123* (13), 8347-8394. https://doi.org/10.1021/acs.chemrev.2c00880.
(33) Takeda, S.; Kuwauchi, Y.; Yoshida, H. Environmental Transmission Electron Microscopy for Catalyst Materials Using a Spherical Aberration Corrector. *Ultramicroscopy* **2015**, *151*, 178-190. https://doi.org/10.1016/j.ultramic.2014.11.017.
(34) Zhao, H.; Zhu, Y.; Ye, H.; He, Y.; Li, H.; Sun, Y.; Yang, F.; Wang, R. Atomic-Scale Structure Dynamics of Nanocrystals Revealed by in Situ and Environmental Transmission Electron Microscopy. *Adv. Mater.* **2023**, *35* (50), 2206911. https://doi.org/10.1002/adma.202206911.
(35) Jinschek, J. Advances in the Environmental Transmission Electron Microscope (ETEM) for Nanoscale in Situ Studies of Gas–Solid Interactions. *Chem. Commun.* **2014**, *50* (21), 2696-2706. DOI: 10.1039/C3CC49092K.
(36) Chee, S. W.; Lunkenbein, T.; Schlögl, R.; Cuenya, B. R. In Situ and Operando Electron Microscopy in Heterogeneous Catalysis—Insights into Multi-Scale Chemical Dynamics. *J. Phys.: Condens. Matter* **2021**, *33* (15), 153001. DOI 10.1088/1361-648X/abddfd.
(37) Tao, F.; Crozier, P. A. Atomic-Scale Observations of Catalyst Structures under Reaction Conditions and During Catalysis. *Chem. Rev.* **2016**, *116* (6), 3487-3539. https://doi.org/10.1021/cr5002657.
(38) Pu, Y.; He, B.; Niu, Y.; Liu, X.; Zhang, B. Chemical Electron Microscopy (CEM) for Heterogeneous Catalysis at Nano: Recent Progress and Challenges. *Res.* **2023**, *6*, 0043. DOI: 10.34133/research.0043.

(39) Su, D. S.; Zhang, B.; Schlögl, R. Electron Microscopy of Solid Catalysts□Transforming from a Challenge to a Toolbox. *Chem. Rev.* **2015**, *115* (8), 2818-2882. https://doi.org/10.1021/cr500084c.
(40) Li, Y.; Ning, Q.; Xu, H.; Li, S.; Wang, J.; Wang, L.; Chen, S.; Zhang, S.; Wang, J.; Hu, Z. Imaging Gas-Involved Structural Dynamics by Environmental Electron Microscopy. *Small* **2025**, 2411415. https://doi.org/10.1002/smll.202411415.
(41) Yuan, W.; Fang, K.; You, R.; Zhang, Z.; Wang, Y. Toward in Situ Atomistic Design of Catalytic Active Sites via Controlled Atmosphere Transmission Electron Microscopy. *Acc. Mater. Res.* **2023**, *4* (3), 275-286. https://doi.org/10.1021/accountsmr.2c00121.
(42) Boyes, E. D.; LaGrow, A. P.; Ward, M. R.; Martin, T. E.; Gai, P. L. Visualizing Single Atom Dynamics in Heterogeneous Catalysis Using Analytical in Situ Environmental Scanning Transmission Electron Microscopy. *Philos. Trans. R. Soc. A* **2020**, *378* (2186), 20190605. https://doi.org/10.1098/rsta.2019.0605.
(43) Wagner, J. B.; Cavalca, F.; Damsgaard, C. D.; Duchstein, L. D.; Hansen, T. W. Exploring the Environmental Transmission Electron Microscope. *Micron* **2012**, *43* (11), 1169-1175. https://doi.org/10.1016/j.micron.2012.02.008.
(44) De Jonge, N.; Ross, F. M. Electron Microscopy of Specimens in Liquid. *Nat. Nanotechnol.* **2011**, *6* (11), 695-704. https://doi.org/10.1038/nnano.2011.161.
(45) Ring, E. A.; De Jonge, N. Microfluidic System for Transmission Electron Microscopy. *Microsc. Microanal.* **2010**, *16* (5), 622-629. doi:10.1017/S1431927610093669.
(46) Chen, X.; Li, C.; Li, B.; Ying, Y.; Ye, S.; Zakharov, D. N.; Hwang, S.; Fang, J.; Wang, G.; Hu, Y.-J. Surface Self-Diffusion Induced Sintering of Nanoparticles. *ACS nano* **2024**, *18* (45), 31160-31173. https://doi.org/10.1021/acsnano.4c09056.
(47) Chen, X.; Zhang, S.; Li, C.; Liu, Z.; Sun, X.; Cheng, S.; Zakharov, D. N.; Hwang, S.; Zhu, Y.; Fang, J. Composition-Dependent Ordering Transformations in Pt–Fe Nanoalloys. *Proc. Natl. Acad. Sci. U.S.A.* **2022**, *119* (14), e2117899119. https://doi.org/10.1073/pnas.2117899119.
(48) Altantzis, T.; Lobato, I.; De Backer, A.; Béché, A.; Zhang, Y.; Basak, S.; Porcu, M.; Xu, Q.; Sánchez-Iglesias, A.; Liz-Marzán, L. M. Three-Dimensional Quantification of the Facet Evolution of Pt Nanoparticles in a Variable Gaseous Environment. *Nano Lett.* **2018**, *19* (1), 477-481. https://doi.org/10.1021/acs.nanolett.8b04303.
(49) Chee, S. W.; Arce-Ramos, J. M.; Li, W.; Genest, A.; Mirsaidov, U. Structural Changes in Noble Metal Nanoparticles during CO Oxidation and Their Impact on Catalyst Activity. *Nat. Commun.* **2020**, *11* (1), 2133. https://doi.org/10.1038/s41467-020-16027-9.
(50) Sun, X.; Zhu, W.; Wu, D.; Li, C.; Wang, J.; Zhu, Y.; Chen, X.; Boscoboinik, J. A.; Sharma, R.; Zhou, G. Surface-Reaction Induced Structural Oscillations in the Subsurface. *Nat. Commun.* **2020**, *11* (1), 305. https://doi.org/10.1038/s41467-019-14167-1.
(51) Sun, X.; Wu, D.; Zou, L.; House, S. D.; Chen, X.; Li, M.; Zakharov, D. N.; Yang, J. C.; Zhou, G. Dislocation-Induced Stop-and-Go Kinetics of Interfacial Transformations. *Nature* **2022**, *607* (7920), 708-713. https://doi.org/10.1038/s41586-022-04880-1.
(52) Sun, X.; Wu, D.; Saidi, W. A.; Zhu, W.; Yang, W. C. D.; House, S. D.; Li, M.; Sharma, R.; Yang, J. C.; Zhou, G. Atomic Dynamics of Multi-Interfacial Migration and Transformations. *Small* **2024**, *20* (11), 2305746. https://doi.org/10.1002/smll.202305746.

(53) Zou, L.; Li, J.; Zakharov, D.; Stach, E. A.; Zhou, G. In Situ Atomic-Scale Imaging of the Metal/Oxide Interfacial Transformation. *Nat. Commun* **2017**, *8* (1), 307. https://doi.org/10.1038/s41467-017-00371-4.
(54) Beck, A.; Huang, X.; Artiglia, L.; Zabilskiy, M.; Wang, X.; Rzepka, P.; Palagin, D.; Willinger, M.-G.; van Bokhoven, J. A. The Dynamics of Overlayer Formation on Catalyst Nanoparticles and Strong Metal-Support Interaction. *Nat. Commun* **2020**, *11* (1), 3220. https://doi.org/10.1038/s41467-020-17070-2.
(55) Frey, H.; Beck, A.; Huang, X.; van Bokhoven, J. A.; Willinger, M.-G. Dynamic Interplay between Metal Nanoparticles and Oxide Support under Redox Conditions. *Science* **2022**, *376* (6596), 982-987. DOI: 10.1126/science.abm3371.
(56) Wu, D.; Sun, X.; Yang, J. C.; Zhou, G. Intermittent Oxidation Kinetics and Metal/Oxide Interfacial Undulation. *Phys. Rev. B* **2024**, *110* (8), 085402. https://doi.org/10.1103/PhysRevB.110.085402.
(57) Monai, M.; Jenkinson, K.; Melcherts, A. E.; Louwen, J. N.; Irmak, E. A.; Van Aert, S.; Altantzis, T.; Vogt, C.; van der Stam, W.; Duchoň, T. Restructuring of Titanium Oxide Overlayers over Nickel Nanoparticles during Catalysis. *Science* **2023**, *380* (6645), 644-651. DOI: 10.1126/science.adf6984.
(58) Zhang, H.; Sun, H.; Shen, K.; Hu, J.; Hu, J.; Jiang, Z.; Song, F. Recent Progress with in Situ Characterization of Interfacial Structures under a Solid–Gas Atmosphere by HP-STM and AP-XPS. *Materials* **2019**, *12* (22), 3674. https://doi.org/10.3390/ma12223674.
(59) Xu, Y.; An, Z.; Tang, Y. Recent Progress in Exploring Heterogeneous Catalyst Surface Chemistry with Near Ambient Pressure XPS. *Sci. China Chem.* **2025**, 1-25. https://doi.org/10.1007/s11426-024-2400-8.
(60) Han, Y.; Zhang, H.; Yu, Y.; Liu, Z. In Situ Characterization of Catalysis and Electrocatalysis Using APXPS. *ACS Catal.* **2021**, *11* (3), 1464-1484. https://doi.org/10.1021/acscatal.0c04251.
(61) Qian, J.; Baskin, A.; Liu, Z.; Prendergast, D.; Crumlin, E. J. Addressing the Sensitivity of Signals from Solid/Liquid Ambient Pressure XPS (APXPS) Measurement. *J. Chem. Phys.* **2020**, *153* (4), 044709. https://doi.org/10.1063/5.0006242.
(62) Schnadt, J.; Knudsen, J.; Johansson, N. Present and New Frontiers in Materials Research by Ambient Pressure X-Ray Photoelectron Spectroscopy. *J. Phys. Condens. Matter* **2020**, *32* (41), 413003. DOI: 10.1088/1361-648X/ab9565.
(63) Cui, Y.; Liao, Y.; Sun, Y.; Wang, W.; Wu, J.; Dai, W.; Huang, T. Advanced XPS-Based Techniques in the Characterization of Catalytic Materials: A Mini-Review. *Catalysts* **2024**, *14* (9), 595. https://doi.org/10.3390/catal14090595.
(64) Lian, X.; Gao, J.; Ding, Y.; Liu, Y.; Chen, W. Unraveling Catalytic Reaction Mechanism by in Situ Near Ambient Pressure X-Ray Photoelectron Spectroscopy. *J. Phys. Chem. Lett.* **2022**, *13* (35), 8264-8277. https://doi.org/10.1021/acs.jpclett.2c01191.
(65) Zhang, H.; Li, X.; Han, Y.; Liu, Z. Direct Work Function Measurement Using In-Situ APXPS and Its Application on Copper Oxidation Process. *Chemphyschem* **2024**, e202300838-e202300838. https://doi.org/10.1002/cphc.202300838.
(66) Goodwin, C. M.; Shipilin, M.; Albertin, S.; Hejral, U.; Lömker, P.; Wang, H.-Y.; Blomberg, S.; Degerman, D.; Schlueter, C.; Nilsson, A. The Structure of the Active Pd State

748 during Catalytic Carbon Monoxide Oxidization. *J. Phys. Chem. Lett.* **2021**, *12* (18),
749 4461-4465. https://doi.org/10.1021/acs.jpclett.1c00620.
750 (67) Zhu, Y.; Wang, J.; Patel, S. B.; Li, C.; Head, A. R.; Boscoboinik, J. A.; Zhou, G. Tuning
751 the Surface Reactivity of Oxides by Peroxide Species. *Proc. Natl. Acad. Sci. U.S.A.* **2023**,
752 *120* (13), e2215189120. https://doi.org/10.1073/pnas.2215189120.
753 (68) Liu, Z.; Huang, E.; Orozco, I.; Liao, W.; Palomino, R. M.; Rui, N.; Duchoň, T.; Nemšák,
754 S.; Grinter, D. C.; Mahapatra, M. Water-Promoted Interfacial Pathways in Methane Oxidation
755 to Methanol on a CeO_2-Cu_2O Catalyst. *Science* **2020**, *368* (6490), 513-517. DOI:
756 10.1126/science.aba5005.
757 (69) Wang, J.; Chen, X.; Li, C.; Zhu, Y.; Li, J.; Shan, S.; Wu, Y.; Hunt, A.; Waluyo, I.;
758 Boscoboinik, J. A. Enhancing Stability of Surface Au under Oxidizing Conditions through
759 Reduced Bulk Au Content. *J. Phys. Chem. Lett.* **2024**, *15* (42), 10583-10591.
760 https://doi.org/10.1021/acs.jpclett.4c02172.
761 (70) Amann, P.; Klötzer, B.; Degerman, D.; Köpfle, N.; Götsch, T.; Lömker, P.; Rameshan, C.;
762 Ploner, K.; Bikaljevic, D.; Wang, H.-Y. The State of Zinc in Methanol Synthesis over a
763 Zn/ZnO/Cu (211) Model Catalyst. *Science* **2022**, *376* (6593), 603-608. DOI:
764 10.1126/science.abj7747.
765 (71) Peng, X.; Zhang, R.; Mi, Y.; Wang, H. T.; Huang, Y. C.; Han, L.; Head, A. R.; Pao, C. W.;
766 Liu, X.; Dong, C. L. Disordered Au Nanoclusters for Efficient Ammonia Electrosynthesis.
767 *ChemSusChem* **2023**, *16* (7), e202201385. https://doi.org/10.1002/cssc.202201385.
768 (72) Diulus, J. T.; Naclerio, A. E.; Boscoboinik, J. A.; Head, A. R.; Strelcov, E.; Kidambi, P.
769 R.; Kolmakov, A. Operando XPS for Plasma Process Monitoring: A Case Study on the
770 Hydrogenation of Copper Oxide Confined under h-BN. *J. Phys. Chem. C* **2024**, *128* (18),
771 7591-7600. https://doi.org/10.1021/acs.jpcc.4c00253.
772 (73) Goodwin, C. M.; Lömker, P.; Degerman, D.; Davies, B.; Shipilin, M.; Garcia-Martinez,
773 F.; Koroidov, S.; Katja Mathiesen, J.; Rameshan, R.; Rodrigues, G. L. Operando Probing of
774 the Surface Chemistry During the Haber–Bosch Process. *Nature* **2024**, *625* (7994), 282-286.
775 https://doi.org/10.1038/s41586-023-06844-5.
776 (74) Shalom, B.-O.; Andrés, M. A.; Head, A. R.; Epstein, B. Z.; Brontvein, O.; Pérez-Dieste,
777 V.; Villar-Garcia, I. J.; Walton, A. S.; Polus, K.; Weatherup, R. S. Chemical State of Nickel
778 Nanoparticles during the Oxygen Evolution Reaction in a Carbonate-Bicarbonate Buffer
779 Solution. *Cell Rep. Phys. Sci.* **2024**, *5* (9), 102165. DOI: 10.1016/j.xcrp.2024.102165.
780 (75) Rämisch, L.; Temperton, R.; Gericke, S. M.; Pfaff, S.; Shavorskiy, A.; Lundgren, E.;
781 Zetterberg, J.; García-Martínez, F. Multi Modal Time-Resolved Infrared and X-Ray
782 Spectroscopic Operando Studies of the CO Oxidation and NO Reduction Reactions on Rh
783 (111). *Appl. Surf. Sci.* **2025**, *687*, 161989. https://doi.org/10.1016/j.apsusc.2024.161989.
784 (76) Yang, J.; Zheng, J.; Dun, C.; Falling, L. J.; Zheng, Q.; Chen, J. L.; Zhang, M.; Jaegers, N.
785 R.; Asokan, C.; Guo, J. Unveiling Highly Sensitive Active Site in Atomically Dispersed Gold
786 Catalysts for Enhanced Ethanol Dehydrogenation. *Angew. Chem. Int. Ed.* **2024**, *63* (35),
787 e202408894. https://doi.org/10.1002/anie.202408894.
788 (77) Yuan, W.; Chen, B.; Han, Z.-K.; You, R.; Jiang, Y.; Qi, R.; Li, G.; Wu, H.;
789 Ganduglia-Pirovano, M. V.; Wang, Y. Direct In-Situ Insights into the Asymmetric Surface
790 Reconstruction of Rutile TiO_2 (110). *Nat. Commun.* **2024**, *15* (1), 1616.
791 https://doi.org/10.1038/s41467-024-46011-6.

(78) Jenkinson, K.; Spadaro, M. C.; Golovanova, V.; Andreu, T.; Morante, J. R.; Arbiol, J.; Bals, S. Direct Operando Visualization of Metal Support Interactions Induced by Hydrogen Spillover During CO_2 Hydrogenation. *Adv. Mater.* **2023**, *35* (51), 2306447. https://doi.org/10.1002/adma.202306447.
(79) Sial, A.; Gao, T.; Dong, Q.; Li, X.; Ren, H.; Liang, X.; Cui, Y.; Wang, C. Advancements in In-Situ Transmission Electron Microscopy for Comprehensive Analysis of Heterogeneous Catalysis: Insights into the Nanoscale Dynamic Processes. *Sci. China Mater.* **2025**, *68*, 39-64. https://doi.org/10.1007/s40843-024-3131-8.
(80) Carvalho, O. Q.; Crumlin, E. J.; Stoerzinger, K. A. X-Ray and Electron Spectroscopy of (Photo) Electrocatalysts: Understanding Activity through Electronic Structure and Adsorbate Coverage. *J. Vac. Sci. Technol. A* **2021**, *39* (4), 040802. https://doi.org/10.1116/6.0001091.
(81) Song, D.; Lin, Y.; Fang, S.; Li, Y.; Zhao, K.; Chen, X.; Huang, Z.; He, F.; Zhao, Z.; Huang, H. Unraveling the Atomic Interdiffusion Mechanism of $NiFe_2O_4$ Oxygen Carriers during Chemical Looping CO_2 Conversion. *Carbon Energy* **2024**, *6* (8), e493. https://doi.org/10.1002/cey2.493.
(82) Li, G.; Zakharov, D. N.; Hu, T.; Yu, Y.; Waluyo, I.; Hunt, A.; Head, A. R.; Boscoboinik, J. A. Tracking the Dynamics of Catalytic Pt/CeO_2 Active Sites during Water-Gas-Shift Reaction. *Commun. Mater.* **2024**, *5* (1), 133. https://doi.org/10.1038/s43246-024-00575-4.
(83) Li, G.; Zakharov, D. N.; Sikder, S.; Xu, Y.; Tong, X.; Dimitrakellis, P.; Boscoboinik, J. A. In Situ Monitoring of Non-Thermal Plasma Cleaning of Surfactant Encapsulated Nanoparticles. *Nanomaterials* **2024**, *14* (3), 290. https://doi.org/10.3390/nano14030290.
(84) Liu, P.; Klyushin, A.; Chandramathy Surendran, P.; Fedorov, A.; Xie, W.; Zeng, C.; Huang, X. Carbon Encapsulation of Supported Metallic Iridium Nanoparticles: An in Situ Transmission Electron Microscopy Study and Implications for Hydrogen Evolution Reaction. *ACS nano* **2023**, *17* (23), 24395-24403. https://doi.org/10.1021/acsnano.3c10850.
(85) Chen, X.; Shan, W.; Wu, D.; Patel, S. B.; Cai, N.; Li, C.; Ye, S.; Liu, Z.; Hwang, S.; Zakharov, D. N. Atomistic Mechanisms of Water Vapor–Induced Surface Passivation. *Sci. Adv.* **2023**, *9* (44), eadh5565. DOI: 10.1126/sciadv.adh5565.
(86) Foucher, A. C.; Lee, J. D.; Qi, Z.; Li, G.; Ouyang, G.; Cui, J.; Boscoboinik, J. A.; Friend, C. M.; Biener, J.; Stach, E. A. Boosting the H_2–D_2 Exchange Activity of Dilute Nanoporous Ti–Cu Catalysts through Oxidation–Reduction Cycle–Induced Restructuring. *Adv. Eng. Mater.* **2023**, *25* (9), 2201724. https://doi.org/10.1002/adem.202201724.
(87) Lin, L.; Liu, J.; Liu, X.; Gao, Z.; Rui, N.; Yao, S.; Zhang, F.; Wang, M.; Liu, C.; Han, L. Reversing Sintering Effect of Ni Particles on γ-Mo_2N via Strong Metal Support Interaction. *Nat. Commun.* **2021**, *12* (1), 6978. https://doi.org/10.1038/s41467-021-27116-8.
(88) Janvelyan, N.; van Spronsen, M. A.; Wu, C. H.; Qi, Z.; Montemore, M. M.; Shan, J.; Zakharov, D. N.; Xu, F.; Boscoboinik, J. A.; Salmeron, M. B. Stabilization of a Nanoporous NiCu Dilute Alloy Catalyst for Non-Oxidative Ethanol Dehydrogenation. *Catal. Sci. Technol.* **2020**, *10* (15), 5207-5217. DOI: 10.1039/D0CY00683A.
(89) Zou, L.; Cao, P.; Lei, Y.; Zakharov, D.; Sun, X.; House, S. D.; Luo, L.; Li, J.; Yang, Y.; Yin, Q. Atomic-Scale Phase Separation Induced Clustering of Solute Atoms. *Nat. Commun.* **2020**, *11* (1), 3934. https://doi.org/10.1038/s41467-020-17826-w.
(90) Li, Y.; Kottwitz, M.; Vincent, J. L.; Enright, M. J.; Liu, Z.; Zhang, L.; Huang, J.; Senanayake, S. D.; Yang, W.-C. D.; Crozier, P. A. Dynamic Structure of Active Sites in

Ceria-Supported Pt Catalysts for the Water Gas Shift Reaction. *Nat. Commun.* **2021**, *12* (1), 914. https://doi.org/10.1038/s41467-021-21132-4.
(91) Yue, S.; Praveen, C. S.; Klyushin, A.; Fedorov, A.; Hashimoto, M.; Li, Q.; Jones, T.; Liu, P.; Yu, W.; Willinger, M. G.; Huang, X. Redox Dynamics and Surface Structures of an Active Palladium Catalyst during Methane Oxidation. *Nat. Commun* **2024**, *15* (1), 4678. https://doi.org/10.1038/s41467-024-49134-y.
(92) Chen, X.; Wang, J.; Zhu, Y.; Xie, Z.; Ye, S.; Kisslinger, K.; Hwang, S.; Zakharov, D. N.; Zhou, G. Atomistic Origins of Reversible Noncatalytic Gas–Solid Interfacial Reactions. *J. Am. Chem. Soc.* **2023**, *145* (7), 3961-3971. https://doi.org/10.1021/jacs.2c10083.
(93) Chen, X.; Liu, Z.; Wu, D.; Cai, N.; Sun, X.; Zakharov, D. N.; Hwang, S.; Su, D.; Wang, G.; Zhou, G. Passive Oxide Film Growth Observed on the Atomic Scale. *Adv. Mater. Interfaces* **2022**, *9* (11), 2102487. https://doi.org/10.1002/admi.202102487.
(94) Lu, X.; Hwang, S.; He, K. In Situ TEM for Structural and Chemical Evolutions of Bimetallic Pt–Ni Nanoparticles at Elevated Temperatures: Implications for Heterogeneous Catalysis. *ACS Appl. Nano Mater.* **2024**, *7* (13), 15735-15742. https://doi.org/10.1021/acsanm.4c02753.
(95) Karagoz, B.; Carpena-Núñez, J.; Zhu, Y.; Baker, L.; Attenkofer, K.; Maruyama, B.; Stacchiola, D.; Zakharov, D. N.; Head, A. R. Adapting an Electron Microscopy Microheater for Correlated and Time-Resolved Ambient Pressure X-Ray Photoelectron Spectroscopy. *Chem. Mater.* **2023**, *35* (15), 5744-5751. https://doi.org/10.1021/acs.chemmater.3c00615.
(96) Zhang, X.; Han, S.; Zhu, B.; Zhang, G.; Li, X.; Gao, Y.; Wu, Z.; Yang, B.; Liu, Y.; Baaziz, W. Reversible Loss of Core–Shell Structure for Ni–Au Bimetallic Nanoparticles During CO_2 Hydrogenation. *Nat. Catal.* **2020**, *3* (4), 411-417. https://doi.org/10.1038/s41929-020-0440-2.
(97) Yin, Z.-W.; Betzler, S. B.; Sheng, T.; Zhang, Q.; Peng, X.; Shangguan, J.; Bustillo, K. C.; Li, J.-T.; Sun, S.-G.; Zheng, H. Visualization of Facet-Dependent Pseudo-Photocatalytic Behavior of TiO_2 Nanorods for Water Splitting Using in situ Liquid Cell TEM. *Nano Energy* **2019**, *62*, 507-512. https://doi.org/10.1016/j.nanoen.2019.05.068.
(98) Ross, F. M. Opportunities and Challenges in Liquid Cell Electron Microscopy. *Science* **2015**, *350* (6267), aaa9886. DOI: 10.1126/science.aaa9886.
(99) Jiang, N.; Spence, J. C. On the Dose-Rate Threshold of Beam Damage in TEM. *Ultramicroscopy* **2012**, *113*, 77-82. https://doi.org/10.1016/j.ultramic.2011.11.016.
(100) Chen, Q.; Dwyer, C.; Sheng, G.; Zhu, C.; Li, X.; Zheng, C.; Zhu, Y. Imaging Beam-Sensitive Materials by Electron Microscopy. *Adv. Mater.* **2020**, *32* (16), 1907619. https://doi.org/10.1002/adma.201907619.
(101) Shen, B.; Wang, H.; Xiong, H.; Chen, X.; Bosch, E. G.; Lazić, I.; Qian, W.; Wei, F. Atomic Imaging of Zeolite-Confined Single Molecules by Electron Microscopy. *Nature* **2022**, *607* (7920), 703-707. https://doi.org/10.1038/s41586-022-04876-x.
(102) Krishna, D. N. G.; Philip, J. Review on Surface-Characterization Applications of X-Ray Photoelectron Spectroscopy (XPS): Recent Developments and Challenges. *Appl. Surf. Sci. Adv.* **2022**, *12*, 100332. https://doi.org/10.1016/j.apsadv.2022.100332.
(103) Tao, F.; Tang, Y. Case Studies: Near Ambient Pressure (NAP) X-Ray Photoelectron Spectroscopy (XPS). In *Springer Handbook of Advanced Catalyst Characterization*, Springer: Cham, **2023**; pp 347-355. https://doi.org/10.1007/978-3-031-07125-6_17.

(104) Weatherup, R. S.; Eren, B.; Hao, Y.; Bluhm, H.; Salmeron, M. B. Graphene Membranes for Atmospheric Pressure Photoelectron Spectroscopy. *J. Phys. Chem. Lett.* **2016**, *7* (9), 1622-1627. https://doi.org/10.1021/acs.jpclett.6b00640.
(105) Tao, F.; Nguyen, L.; Amati, M.; Gregoratti, L. Preparation of a Membrane-sealed Cell for Studying Catalyst Nanoparticles in Flowing Gas with High Vacuum X-Ray Photoelectron Spectrometer. *Rev. Sci. Instrum.* ***2024***, *95* (5), 055108. https://doi.org/10.1063/5.0186088.
(106) Huang, B.; Wu, Z.; Zhou, H.; Li, J.; Zhou, C.; Xiong, Z.; Pan, Z.; Yao, G.; Lai, B. Recent Advances in Single-Atom Catalysts for Advanced Oxidation Processes in Water Purification. *J. Hazard. Mater.* ***2021***, *412* (15), 125253. https://doi.org/10.1016/j.jhazmat.2021.125253.
(107) Jiang, K.; Siahrostami, S.; Zheng, T.; Hu, Y.; Hwang, S.; Stavitski, E.; Peng, Y.; Dynes, J.; Gangisetty, M.; Su, D.; Attenkofer, K. Isolated Ni Single Atoms in Graphene Nanosheets for High-Performance CO_2 reduction. *Energy Environ. Sci.* ***2018***, *11* (4), 893-903. DOI: 10.1039/C7EE03245E.
(108) Su, W.; Cheng, X.; Shang, S.; Pan, R.; Qi, M.; Sang, Q.; Xie, Z.; Zhang, H.; Wang, K.; Liu, Y. Advances in In Situ Investigations of Heterogeneous Catalytic Ammonia Synthesis. *Catalysts* ***2025****, 15* (2), 160. https://doi.org/10.3390/catal15020160.
(109) Nguyen, L.; Tao, P.P.; Liu, H.; Al-Hada, M.; Amati, M.; Sezen, H.; Gregoratti, L.; Tang, Y.; House, S.D.; Tao, F.F. X-ray Photoelectron Spectroscopy Studies of Nanoparticles Dispersed in Static Liquid. *Langmuir* ***2018****,34* (33), 9606-9616. https://doi.org/10.1021/acs.langmuir.8b00806.